Ultrasonics Sonochemistry 86 (2022) 106008

Contents lists available at ScienceDirect

Ultrasonics Sonochemistry

journal homepage: www.elsevier.com/locate/ultson

Study on a novel omnidirectional ultrasonic cavitation removal system for Microcystis aeruginosa

Hao-Ren Feng [a,1], Jian-An Wang [a,b,1], Liang Wang [a,*], Jia-Mei Jin [a], Shu-Wen Wu [c], Charles-C. Zhou [c]

[a] State Key Laboratory of Mechanics and Control of Mechanical Structures, Nanjing University of Aeronautics and Astronautics, Yudao 29, Nanjing 210016, China
[b] AVIC Taiyuan Aero-Instruments Co., Ltd., Taiyuan 030006, China
[c] Zhejiang Refine Environmental Technology, Corp. Ltd., Wenzhou 325024, China

ARTICLE INFO

Keywords:
Ultrasonic algae removal system
Ultrasonic cavitation
Bending vibration
Ultrasonic transducer
Microcystis aeruginosa

ABSTRACT

Microcystis aeruginosa, as a typical alga, produces microcystin with strong liver toxicity, seriously endangering the liver health of human and animals. Inhibiting the bloom of the Microcystis aeruginosa in lakes becomes a significant and meaningful work. Ultrasonic cavitation is currently considered to be the most environmentally friendly and effective method for the removal of Microcystis aeruginosa. However, the commercialized ultrasonic algae removal systems require multi-Langevin transducers to achieve omnidirectional ultrasonic irradiation due to the single irradiation direction of the Langevin transducer, resulting in the complex design and high energy consumption. To achieve a low-cost, simple structure, and high-efficiency algae removal system, a novel omnidirectional ultrasonic cavitation removal system for Microcystis aeruginosa is proposed. The proposed system is major composed of a novel omnidirectional ultrasonic transducer, which generates the omnidirectional ultrasonic irradiation by its shaking-head motion coupled by two orthogonal bending vibration modes. Modal simulation, sound field simulation, and cavitation bubble radius simulation are first carried out to optimize the geometric sizes of the proposed transducer and verify the correctness of the omnidirectional ultrasonic irradiation principle. Then the vibration characteristics of the transducer prototype are measured by vibration tests and impedance tests. Finally, the feasibility and effectiveness of the proposed omnidirectional ultrasonic removal system for Microcystis aeruginosa are evaluated through the algae removal experiments. The experimental results exhibit that the algal cells damaged by ultrasonic irradiation from the proposed system do not have the ability to self-repair. In addition, the algal removal rates reached 55.41% and 72.97% after 30 min of ultrasonic treatment when the corresponding ultrasonic densities are 0.014 W/mL and 0.021 W/mL, respectively. The proposed omnidirectional ultrasonic algae removal system significantly simplifies the configuration and reduces energy consumption, presenting the potential promise of algae removal and environmental protection.

1. Introduction

With the rapid development of human industrial civilization, the excessive reproduction of harmful algae in water caused by anthropogenic eutrophication has become a serious problem [1,2]. Algal blooms destroy the ecological balance of the waters, as well as produces harmful algae toxins that endanger the health of humans, livestock, and aquatic ecosystems. In particular, Microcystis aeruginosa (M. aeruginosa) produces microcystin with strong liver toxicity. Long-term drinking of water containing microcystin may cause liver and gallbladder lesions [3–7]. Numerous studies have confirmed that biological methods (e.g., microbial degradation), chemical methods (e.g., the addition of oxidants, photocatalytic active materials, and nanocomposite materials), and physical methods (e.g., air flotation, filtration, and flocculation precipitation methods) are effective strategies for reducing cyanobacterial bloom [8-13]. However, these methods present defects in practical applications: biological methods are easily restricted by the external environment and cause biological invasion, the by-products of chemical methods may pollute water quality on the other hand, and physical methods are limited by high cost and low efficiency.

* Corresponding author.
E-mail address: lwang@nuaa.edu.cn (L. Wang).
[1] Hao-Ren Feng and Jian-An Wang are co-first authors of this article.

https://doi.org/10.1016/j.ultsonch.2022.106008
Received 11 February 2022; Received in revised form 11 April 2022; Accepted 15 April 2022
Available online 20 April 2022

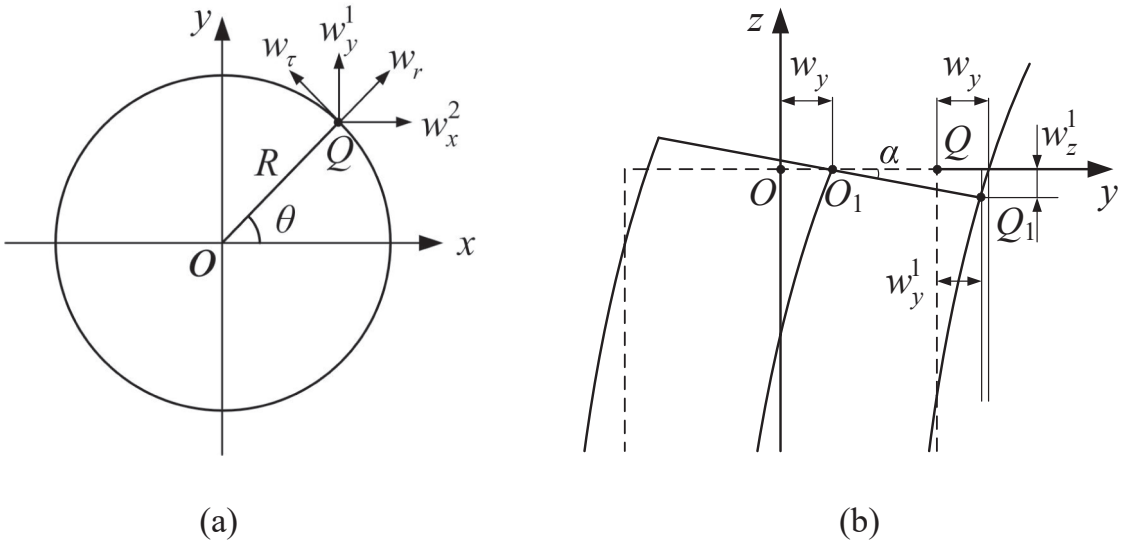

Fig. 1. Schematic diagram of the bending deformation of the end of the transducer. (a) Displacement analysis of point *Q* in X-Y plane. (b) Displacement analysis of point *Q* in Y-Z plane.

Ultrasonic irradiation reduces the biological activity of algae cells through the cavitation effect that occurs inside the cells, thereby inhibiting or controlling the blooming of algae blooms, and is considered as the most environmentally friendly treatment method at present [14-16]. When the sound waves propagate in water, cavitation nucleus are formed inside the algae cells during the alternating process of the expansion and compression phases of the waves [17-19]. With sufficient ultrasonic density, the cavitation nucleus is compressed and exploded after multiple alternating cycles, destroying the gas vesicles in algae cells and interrupting photosynthetic activity [20-22]. Currently, a variety of ultrasonic algae removal devices have been developed and employed [23-25]. Schneider et al. [26] developed an ultrasonic buoy system to control algae growth in a 200-acre reservoir, which significantly improved the water quality. Lee et al. [27] established a 200 kHz ultrasonic irradiation system to destroy the vacuoles of cyanobacteria in Senba Lake to prevent algae blooms. The MPC-Buoy algae removal instrument developed by LG-SONIC in the Netherlands is widely used in the New Jersey Reservoir of the United States, the cooling pool of the Raphael Nuclear Power Plant in the United Kingdom, the Dubai City Government Sightseeing Lake, etc. [23]. The algae removal systems mentioned above usually use Langevin ultrasonic transducers as the ultrasonic generator. Due to the irradiation direction of Langevin transducers is limited, multi-Langevin transducers with different orientations are required to achieve omnidirectional ultrasonic irradiation. Nevertheless, this kind of transducer array leads to a complex power supply system and complicated control system, high energy consumption, high cost, and low efficiency. To further improve the efficiency of ultrasonic algae removal and reduce the cost, numerous research institutions mainly focus on studying the influence of ultrasonic frequency, ultrasonic density, irradiation time, and other parameters on the algae removal effect [28-33]. With the optimal ultrasonic parameters, the efficiency of algae removal has been improved to varying degrees. However, as the core reason of the complex configuration and high system cost, the ultrasonic transducer has been little optimized. Especially the transducer capable of omnidirectional ultrasonic irradiation is still a blank at present.

To improve the aforesaid problem, a novel omnidirectional ultrasonic removal system for M. aeruginosa using a single ultrasonic transducer is proposed in this study. Different from traditional ultrasonic algae removal systems, a novel omnidirectional ultrasonic irradiation transducer (OUAT) with bending-bending coupled vibration is proposed in this paper. Through the regular arrangement of multiple piezoelectric ceramic (PZT) plates, two spatially orthogonal first-order bending vibrations are excited and coupled in the OUAT, presenting the head-shaking movements at both ends of the transducer. It means that the direction of vibration of the proposed transducer changes continuously along the circumferential direction, leading to the production of omnidirectional ultrasonic irradiation. Hence, the above-mentioned transducer array can be replaced by a single OUAT, simplifying the configuration and control system, improving the energy utilization rate, and reducing the cost.

This paper is organized as follows. The sound pressure distribution, the sound pressure level, and the sound pressure irradiation received by waters at different distances from the proposed OUAT are first theoretically analyzed and simulated to verify the feasibility of the proposed OUAT with omnidirectional irradiation. Then, the cavitation bubble radius is calculated to reveal the cavitation effect produced by the transducer. Finally, the removal experiments of M. aeruginosa are carried out to evaluate the effectiveness of the proposed OUAT algae system.

2. Design method

2.1. Theoretical analysis

When the sound wave propagates to the liquid, the medium in the negative pressure phase is subjected to a force of $P_h - P$, where P_h represents the hydrostatic pressure, and P is the sound pressure acting on a medium in the sound field. As the sound intensity increases, the distance between the medium molecules increases due to the negative pressure. After the distance exceeds the limitation, the integrity of the liquid structure is destroyed and cavities are generated [34]. On the other hand, the thermal deposition during the acoustic wave transmission also affects the generation of cavitation nuclei in the liquid. The thermal motions within the liquid form temporary and microscopic voids that can constitute the nuclei necessary for the rupture and growth of macroscopic bubbles [35]. Meanwhile, the liquid enters a metastable state when it is stretched beyond its vapor pressure or superheated above the boiling point, at which time the thermal deposition in the liquid facilitates bubble nucleation by lowering the cavitation threshold [36,37].

The cavitation threshold P_c refers to the minimum sound intensity that caused the liquid to create cavitation. In a structurally complete liquid, the threshold sound pressure for generating a cavity with a radius

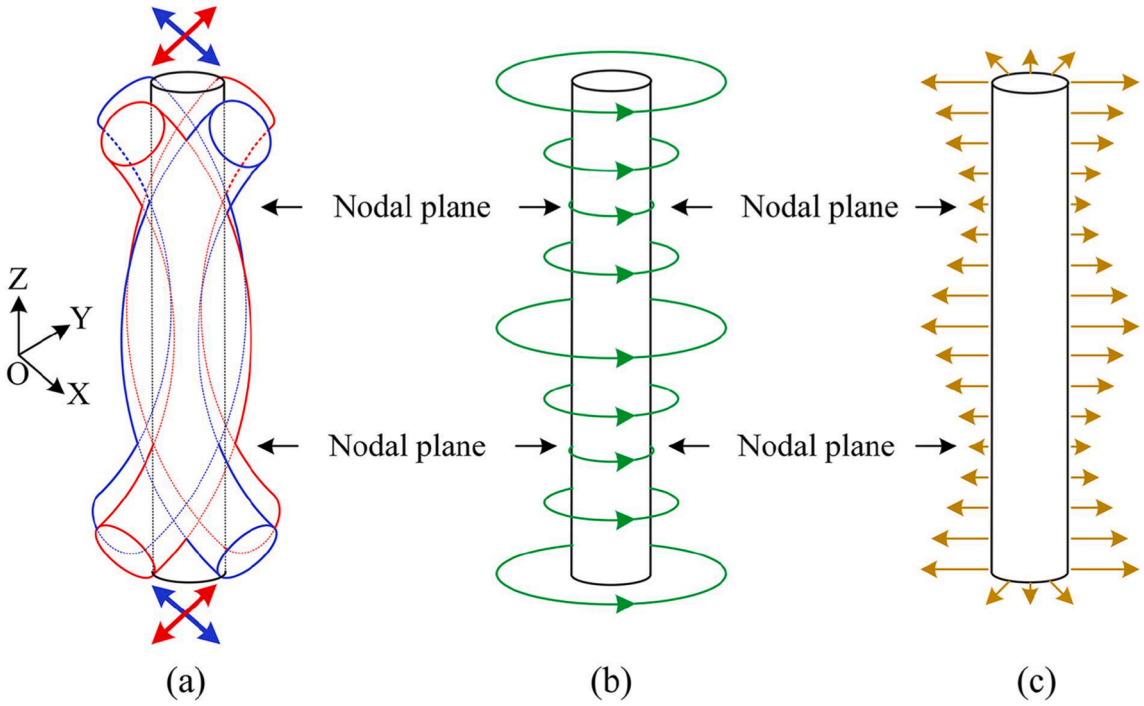

Fig. 2. Working principle of the transducer. (a) Two orthogonal first-order bending vibration modes of the transducer. (b) Shaking-head movements of the transducer coupled by the above two vibration modes. (c) Schematic diagram of the ultrasonic irradiation direction generated by the transducer.

of R_0 is:

$$P_c = P_h - P_v + \frac{2}{3\sqrt{3}}\sqrt{\frac{(2\sigma/R_0)^3}{(P_h - P + 2\sigma/R_0)}} \tag{1}$$

where σ is the surface tension of the liquid, P_v is the vapor pressure. Therefore, the difference in temperature, hydrostatic pressure, and gas content in the same medium leads to different cavitation thresholds. However, the cavitation threshold generally depends on the ultrasound frequency. High ultrasound frequency requires high P_c. In addition, the higher ultrasound intensity applied to the liquid, the easier it is to produce cavities.

Sound intensity, is defined as the power carried by sound waves per unit area in a direction perpendicular to that area, can be expressed as:

$$I = \bar{\varepsilon} c_0 \tag{2}$$

where c_0 is the speed of sound in the medium, and $\bar{\varepsilon}$ is the average sound energy density, which is given as:

$$\bar{\varepsilon} = \frac{p_m^2}{2\rho_0 c_0^2} \tag{3}$$

where ρ_0 is the density of liquid, $p_m = u_m \rho_0 c_0$ represents the amplitude of sound pressure, and u_m is the amplitude of the particle vibration velocity. Hence, the sound intensity propagates along a certain direction can be expressed as:

$$I = \frac{p_m^2}{2\rho_0 c_0} = \frac{1}{2} p_m u_m \tag{4}$$

The aforementioned analyses mean that the sound intensity is proportional to the amplitudes of the sound pressure and the particle vibration velocity, and it is a vector pointing to the direction of the sound propagation.

Therefore, the key to achieving the omnidirectional ultrasonic algae removal is that the ultrasonic transducer can generate the omnidirectional ultrasonic radiation while ensuring the generation of cavitation. This research focused on the design of a mid-frequency ultrasonic transducer with the omnidirectional vibration.

Assuming that the transducer is a cylinder, when two electrical signals with a phase difference of $\pi/2$ are applied to the two groups of PZT plates, two orthogonal bending vibration modes can be excited in the transducer, respectively. The displacement at any point Q on the end face of the transducer in a bending vibration mode is analyze, as shown in Fig. 1. When a sinusoidal voltage of $\sin\omega t$ is applied to a group of the PZT plates, the displacement response w_y of the center point O and the rotation angle response α of the end face are:

$$w_y = w_0 \sin\omega t \tag{5}$$

$$\alpha = \alpha_0 \sin\omega t \tag{6}$$

where w_0 and α_0 are the displacement amplitude and the rotation angle amplitude of point O in the Y direction, respectively.

In the case of small deformation, the bending deformation of the transducer conforms to the plane assumption. As descripted in Fig. 1(b), the displacement responses of the point Q in the Y and Z directions are:

$$w_y^1 = w_y - w_z^1 \tan\alpha = w_0 \sin\omega t - w_z^1 \tan\alpha \tag{7}$$

$$w_z^1 = -R\sin\theta\sin\alpha \approx -R\alpha_0 \sin\theta \sin\omega t \tag{8}$$

Due to the small deformation angle in X-Y plane during the bending vibration, the second term of Eq. (7) $w_z^1 \tan\alpha$ is much smaller than its first term$w_0 \sin\omega t$. Hence, Eq. (7) can be simplified as:

$$w_y^1 \approx w_0 \sin\omega t \tag{9}$$

Similarly, when a sinusoidal voltage of $\cos\omega t$ is applied to another group of the PZT plates, the displacement responses of point Q in the X direction and Z direction are:

$$w_x^2 = w_0 \cos\omega t \tag{10}$$

$$w_z^2 = -R\alpha_0 \cos\theta \cos\omega t \tag{11}$$

When the two electrical signals are applied to the two groups of PZT plates simultaneously, the displacement response of point Q in the Z

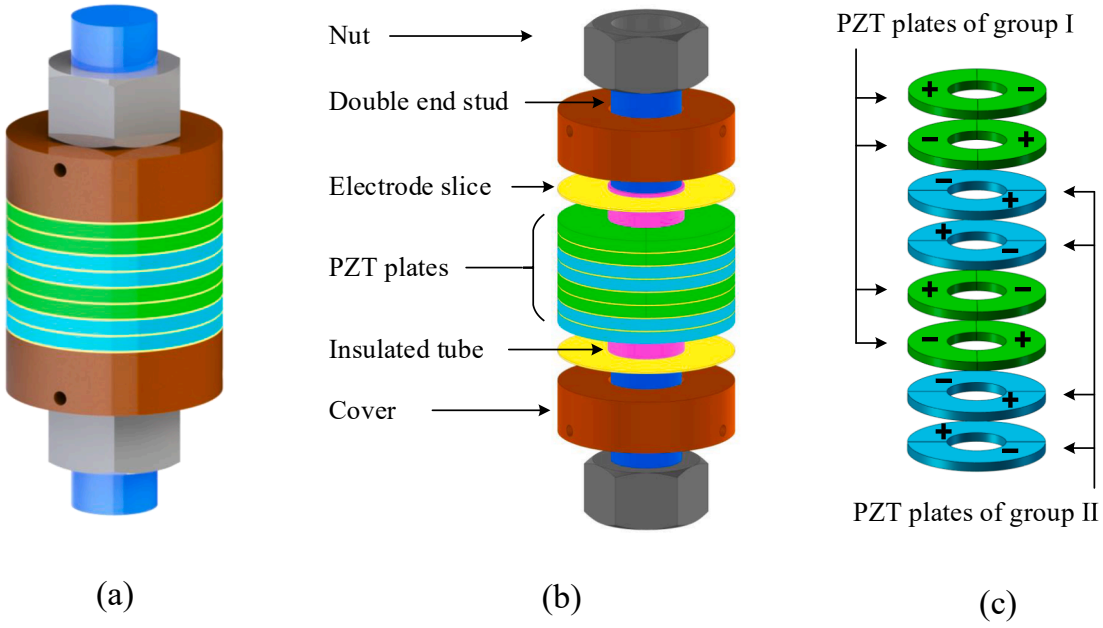

Fig. 3. Configuration view of the proposed OUAT and details. (a) Structure of the OUAT. (b) Exploded view of the OUAT. (c) Polarization directions of PZT plates.

direction is:

$$w_z^{total} = -R\alpha_0(\sin\theta\sin\omega t + \cos\theta\cos\omega t) = -R\alpha_0\cos(\omega t - \theta) \quad (12)$$

As shown in Fig. 1(a), decompose w_y^1 and w_x^2 along the normal and tangential directions of point Q, and the responses of normal displacement w_r and tangential displacement w_τ can be expressed as:

$$w_r = w_y^1\sin\theta + w_x^2\cos\theta = w_0\cos(\omega t - \theta) \quad (13)$$

$$w_\tau = -w_y^1\sin\theta + w_x^2\cos\theta = w_0\sin(\omega t - \theta) \quad (14)$$

Analyzing Eq. (12) can obtain that, the displacement response of point Q in the Z direction is related to the time t and the direction angleθ, which performs a simple harmonic rotating along the circumference of the transducer. It can be known in Eqs. (13) and (14) that the responses of normal and tangential displacements at any point on the end of the transducer conform to the traveling wave equation, which means that the transducer vibrates as shaking its head.

2.2. Transducer working principle and configuration

Since the effective irradiation range of low-frequency ultrasonic waves is larger than that of high-frequency ultrasonic waves [38], low-order vibration modes of the ultrasonic transducer are the preferred option for efficient algae removal. Two orthogonal first-order bending vibration modes are employed to couple the aforementioned shaking-head movement in a cylinder transducer because of its low frequency and large wavelength, as shown in Fig. 2(a). The cylinder formed by the black lines in the figure represents the transducer without vibration, and the deformed transducers under the two vibration modes are represented by the red and blue lines, respectively. The two vibration directions of the cylinder transducer are along the X-axis and Y-axis, respectively. It can be seen that the maximum deformation occurred at the two ends of the transducer and the center of its axis. And there are two nodal planes along the axial direction of the transducer.

The coupled shaking-head movement of the cylinder transducer is indicated in Fig. 2(b). The green arrows denote the directions and shaking amplitudes of the shaking-head movements. Theoretically, at different positions of the transducer, as long as there are vibrations, the shaking-head movement will be coupled here. Therefore, the rest positions of the transducer except for the nodal planes perform the shaking-head movements with different shaking amplitudes according to the vibration amplitudes. From the two ends and the axis center of the transducer to the positions of the nodal planes, the amplitude of the shaking-head movement gradually decreases. According to Eq. (4) can be inferred that the ultrasonic irradiation generated by the transducer at different positions is different, as shown in Fig. 2(c). Yellow arrows represent the directions and magnitudes of the ultrasonic irradiation. The largest ultrasonic irradiation will be generated at the two ends and the axis center of the transducer. In addition, the directions of the ultrasonic irradiation generated by the proposed transducer are consistent with the directions of its shaking-head movements, which means that the directions of the ultrasonic irradiation are constantly changing.

Based on this principle, a novel omnidirectional ultrasonic irradiation transducer is proposed, as illustrated in Fig. 3. Eight PZT plates with dual-polarization zones are regularly arranged among the nine electrode plates, and they are fixed on a double-ended stud by two cylindrical metal covers and two pre-tightening bolts. The purpose of choosing PZT plates with dual-polarization zones is to excite the two orthogonal first-order bending vibration modes of the proposed transducer. There are three threaded holes evenly arranged on the cylindrical surface of each metal cover, and the positions of the threaded holes are located on the nodal plane of the two bending vibration modes.

PZT plates are equally divided into groups I and II according to the spatial distribution of their polarization zones. The two groups of PZT plates have a spatial phase difference of $\pi/2$. It means that the two vibration modes independently excited by these two groups of PZT plates are orthogonal in space. Therefore, when two electrical signals of a specific frequency with a temporal phase difference of $\pi/2$ are, respectively, applied to the two group of PZT plates, a traveling wave rotating along the circumference direction will be coupled at both ends of the double-ended stud, in other word, the OUAT presents a vibrating motion similar to shaking-head.

3. Simulation analysis

3.1. Finite element simulation model

Utilizing the finite element method (FEM) based on the commercial software COMSOL Multiphysics 5.5, the modal analysis and sound field

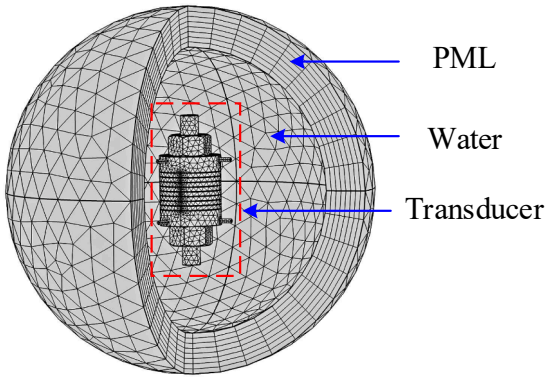

Fig. 4. Sectional stereogram of the simulation meshing model.

simulation were conducted on the OUAT. There are two primary purposes of simulation analysis. On the one hand, the geometrical dimensions of the OUAT can be optimized through modal simulation analysis to reduce the frequency difference of the two orthogonal first-order bending vibration modes. On the other hand, by simulating the underwater working environment of the transducer in reality, the sound characteristics of the OUAT can be correctly analyzed to verify the correctness of the omnidirectional ultrasonic irradiation principle.

To simulate the actual working environment of the OUAT, it was placed in a spherical water area, while the periphery of the water was surrounded by a perfectly matched layer (PML), as shown in Fig. 4. The PML here refers to an infinitely thick water, which can absorb almost all incident waves without reflection. In this simulation model, the element type of the PML was set to a cuboid mesh, and the rest were set to a free tetrahedral mesh. The maximum size of the water element was set to 1/6 of a wavelength to ensure the calculation accuracy of the sound pressure. Meanwhile, eight layers of mesh were divided along the thickness of the PML to ensure the sound wave are absorbed entirely.

The material of the PZT plates is circular ring-shaped PZT-8 with dual-polarization zones (Haiying Company, Wuxi, China), and its outer diameter, inner diameter, and thickness are 30 mm, 13 mm, and 2 mm, respectively. Two cylindrical metal covers, two pre-tightening bolts, and the double-ended stud are made of 304 stainless steels. The electrode plates are silver-plated copper plates with a thickness of 0.30 mm. In particular, a 0.5 mm thick Nylon-PA66 insulating sleeve was placed between the outer surface of the bolt and the inner ring surface of PZT plates and electrode plates, insulating the electrode plate from the double-ended stud, and ensuring the verticality of PZT plates during

Table 1
Material parameters of the OUAT.

Material	304 stainless steels	Copper	Nylon-PA66	PZT-8
Density (kg/m3)	7750	8960	1150	7650
Young's modulus (GPa)	193	110	2	$\begin{pmatrix} 120.6 & 53.5 & 51.5 & 0 & 0 & 0 \\ 53.5 & 120.6 & 51.5 & 0 & 0 & 0 \\ 51.5 & 51.5 & 104.5 & 0 & 0 & 0 \\ 0 & 0 & 0 & 31.3 & 0 & 0 \\ 0 & 0 & 0 & 0 & 31.3 & 0 \\ 0 & 0 & 0 & 0 & 0 & 34.6 \end{pmatrix}$
Poisson's ratio	0.31	0.35	0.4	/
Damping Factor	0.002	0.001	0.15	0.0016
Relative permittivity	1	1	4	$\begin{pmatrix} 904.4 & 0 & 0 \\ 0 & 904.4 & 0 \\ 0 & 0 & 561.6 \end{pmatrix}$
Piezoelectric constant (C/m2)	/	/	/	$\begin{pmatrix} 0 & 0 & -5.2 \\ 0 & 0 & -5.2 \\ 0 & 0 & 15.1 \\ 0 & 0 & 0 \\ 0 & 12.7 & 0 \\ 12.7 & 0 & 0 \end{pmatrix}$

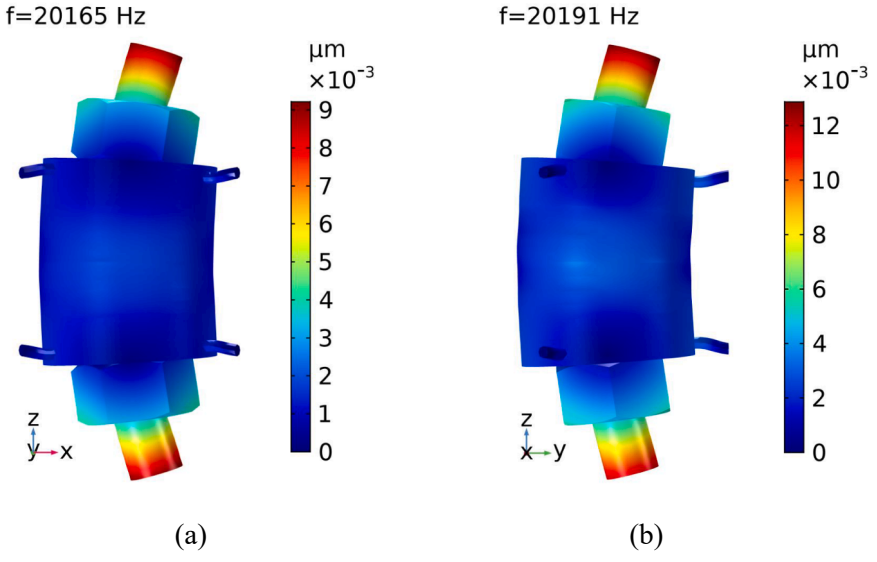

Fig. 5. First-order bending vibration modes of the OUAT in (a) *X-Z* plane (mode A) and (b) Y-Z plane (mode B).

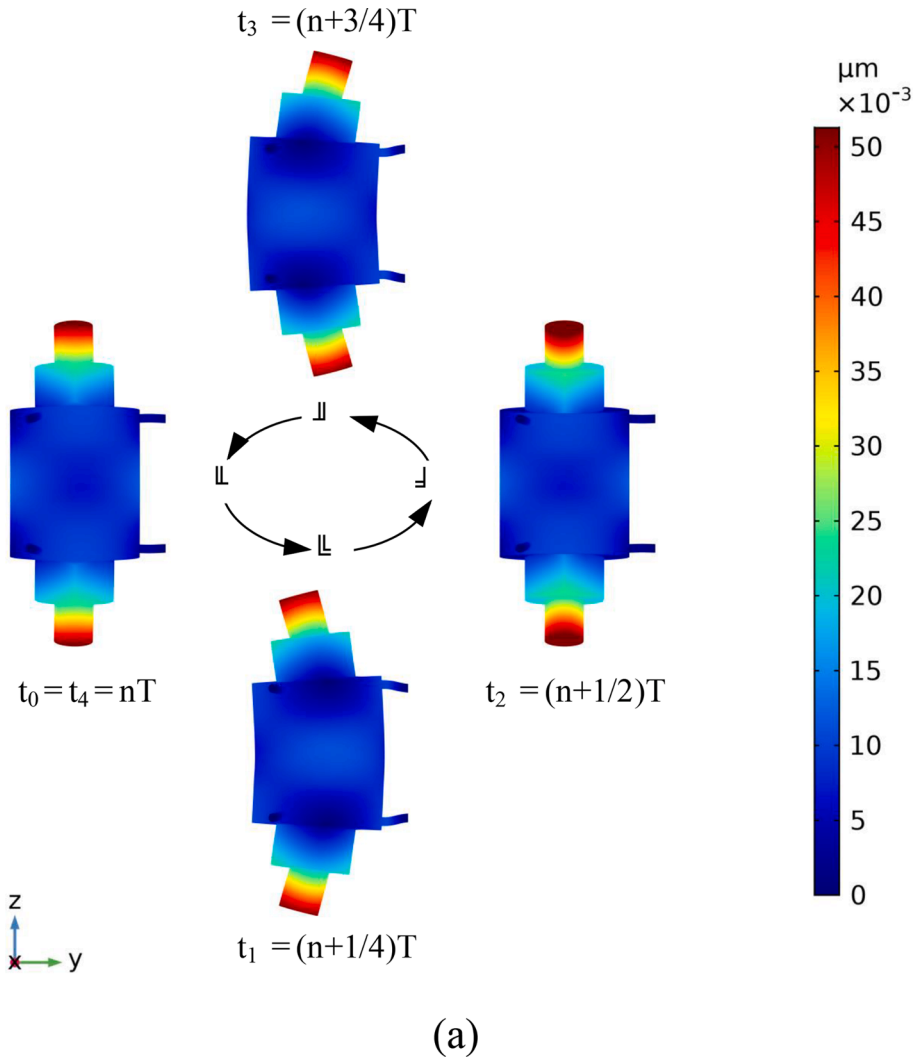

Fig. 6. Shaking-head movement of the OUAT in (a) *X-Z* plane and (b) Y-Z plane. The vibration shape of the OUAT can be seen in supporting information named "1" and "2".

assembly. In addition, six bolts made of Nylon-PA66 were installed in the threaded holes of the cover plate. All material parameters are listed in Table 1. In all simulations in this study, two electrical signals with a peak-to-peak voltage of 1 V (1 V_{PP}) were applied to the electrode plates. The end faces of the six bolts were set as fixed constraints.

3.2. Modal simulation

The calculated working vibration modes of the OUAT are shown in Fig. 5. When an electric signal with a frequency of 20,165 Hz was applied to the PZT plates of group I, the OUAT presented the first-order bending vibration mode in the X-Z plane (mode A). Similarly, the first-order bending vibration mode of the OUAT in the Y-Z plane (mode B) was appeared when an electric signal with a frequency of 20,191 Hz was applied to the PZT plates of group II. Compared with the middle section of the OUAT, two ends of the OUAT have the largest vibration displacement due to the smaller cross-section. The resonant frequency difference between the two working vibration modes is 26 Hz, caused by the clamping of six nylon bolts, indicating that two vibration modes can be coupled into a traveling wave at the both ends of the OUAT.

According to the above simulation results, a harmonic response analysis was conducted to tune the response frequencies of the two working modes. The tuned exciting frequency of the OUAT was 20173 Hz after the harmonic response analysis. Under the excitation of two electric signals with a temporal phase difference of π/2, the optimized vibration shape of the OUAT was obtained, as illustrated in Fig. 6. During one period, the vibration shape changed as ①-②-③-④, as shown in Fig. 5(a). It can be seen that the vibration direction of the OUAT changes with time. Correspondingly, the end face of OUAT shows a shaking-head movement, as shown in Fig. 5(b).

3.3. Sound field simulation

With the above harmonic response analysis, in addition to the vibration shape, the sound field distribution generated by the OUAT vibration was obtained, as shown in Fig. 7. Sound pressure and sound pressure level are essential parameters that characterize the sound characteristics of a algae removal transducer. The sound field distributions of the Y-Z and X-Y sections of the simulation model, that is, in the axial and circumferential directions of the OUAT, are shown in Fig. 7(a) and (b). Since the sound field was only calculated in the water, the display of the OUAT in the simulation nephograms is blank. Along the axis of the OUAT, both ends of the transducer generated a significant sound pressure in the surrounding water due to their maximum vibration speed (seen in supporting information named "3"). Because of the shaking-head motion of the OUAT ends, the produced sound field also

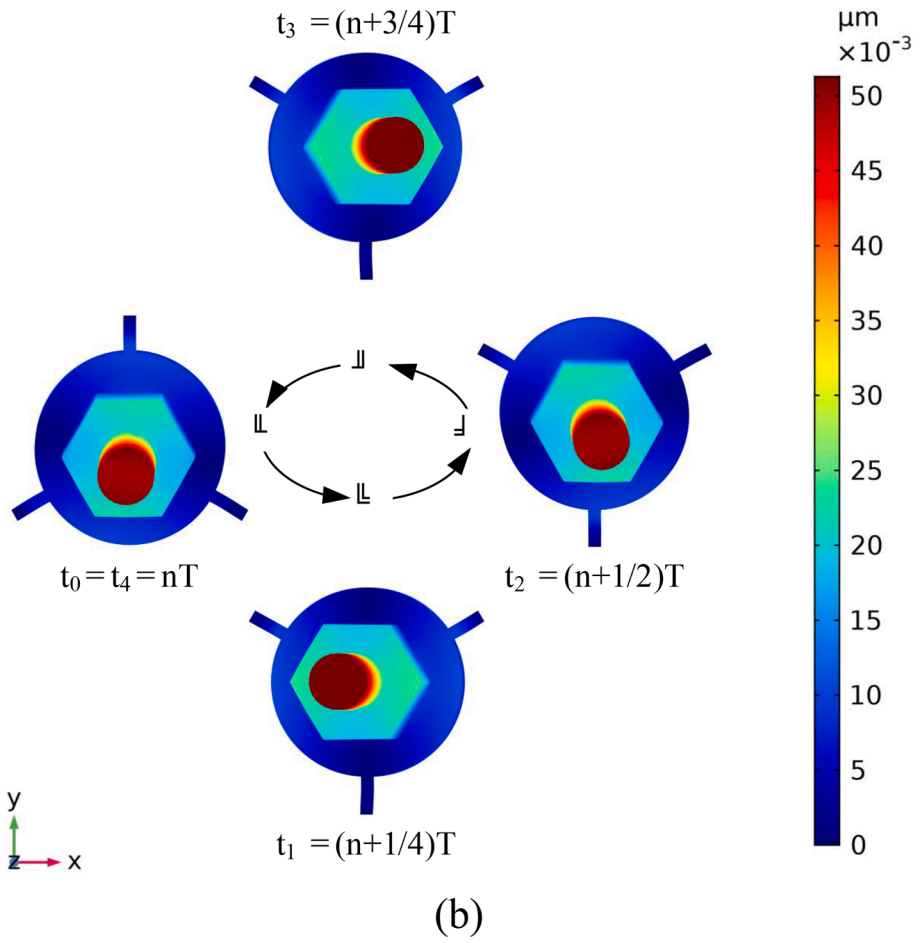

Fig. 6. (*continued*).

changes continuously along the direction of movement, in which the positive pressure zone and the negative pressure zone alternately rotate (seen in supporting information named "4"). The sound pressure levels of the two sections generated by the OUAT vibration are shown in Fig. 7 (c) and (d), which indicate that the proposed transducer can produce a good sound pressure level in water at a voltage of 1 V_{pp}. And the sound pressure level gradually attenuates from the solid–liquid interface of the OUAT to the water area.

To analyze the sound characteristics of the water at different distances from the OUAT, the exterior-field sound pressure level of the water was analyzed and computed, and the results are shown in Fig. 8. The exterior-field refers to the water area with a certain distance in the radial direction of the transducer. Fig. 8 is a polar coordinate diagram of wavenumber sensitivity (Beam pattern), in which the radius coordinate refers to different sound pressure levels, indicating the distribution of sound pressure levels in the water at a distance of 0.1 m, 1 m, and 10 m from the transducer.

The plane of the Beam pattern in Fig. 8(a) coincides with the Y-Z plane of the Cartesian coordinate system in Fig. 7. It can be noted that there is almost no ultrasonic irradiation near the 0° and 180° directions of the OUAT (the axis of OUAT). This is because the main deformation direction of the transducer occurs in the X-Y plane, and the vibration velocity of the OUAT in the *Z* direction is relatively small. The minimum values of ultrasonic irradiation appear in the directions of 75°, 105°, 255° and 285° of the OUAT. These four directions respectively correspond to the node positions of the first-order bending vibration mode. Similarly, the maximum values of ultrasonic irradiation occur in 35°, 145°, 215°, and 325° of the OUAT. These four directions correspond to the maximum amplitude of the first-order bending vibration mode. These prove that the mechanical properties of the ultrasonic transducer directly affect its sound properties. In addition, the maximum sound pressure levels of water at 0.1 m, 1 m, and 10 m from the OUAT are 160 dB, 140 dB, and 110 dB, respectively, indicating that the effect of ultrasonic irradiation gradually weakens as the radial distance increases. The plane of the beam pattern illustrated in Fig. 8(b) coincides with the X-Y plane of the Cartesian coordinate system shown in Fig. 7. The sound pressure level isolines at different distances from the transducer present the perfect circular distribution, indicating that the ultrasonic irradiation generated by the OUAT in the circumferential direction has the same amplitude, further verifying that the proposed transducer has the function of omnidirectional ultrasonic irradiation.

3.4. Ultrasonic cavitation bubble simulation

Assuming the bubble wall in the sound field only moves radially, the bubble is always spherical and the center of the sphere is fixed during the movement. Meanwhile, considering the effects of liquid viscosity and surface tension on the radial velocity of the bubble, the bubble radius equation was defined as [39,40]:

$$R\ddot{R}+\frac{3}{2}\dot{R}^2=\frac{1}{\rho}\left[\left(P_0+\frac{2\sigma}{R_0}\right)\left(\frac{R_0}{R}\right)^{3K}-\frac{2\sigma}{R}-4\mu\frac{\dot{R}}{R}-P_0+P_V+P_a\sin\omega t\right] \tag{15}$$

where R is the instantaneous radius of cavitation bubble, R_0 is the initial radius of the bubble, $\dot{R}$ is the velocity of the particle on the bubble wall, $\ddot{R}$ is the motion acceleration of the particle on the bubble wall, ρ is the liquid density, P_0 is the static liquid pressure, P_v is the vapor pressure, P_a

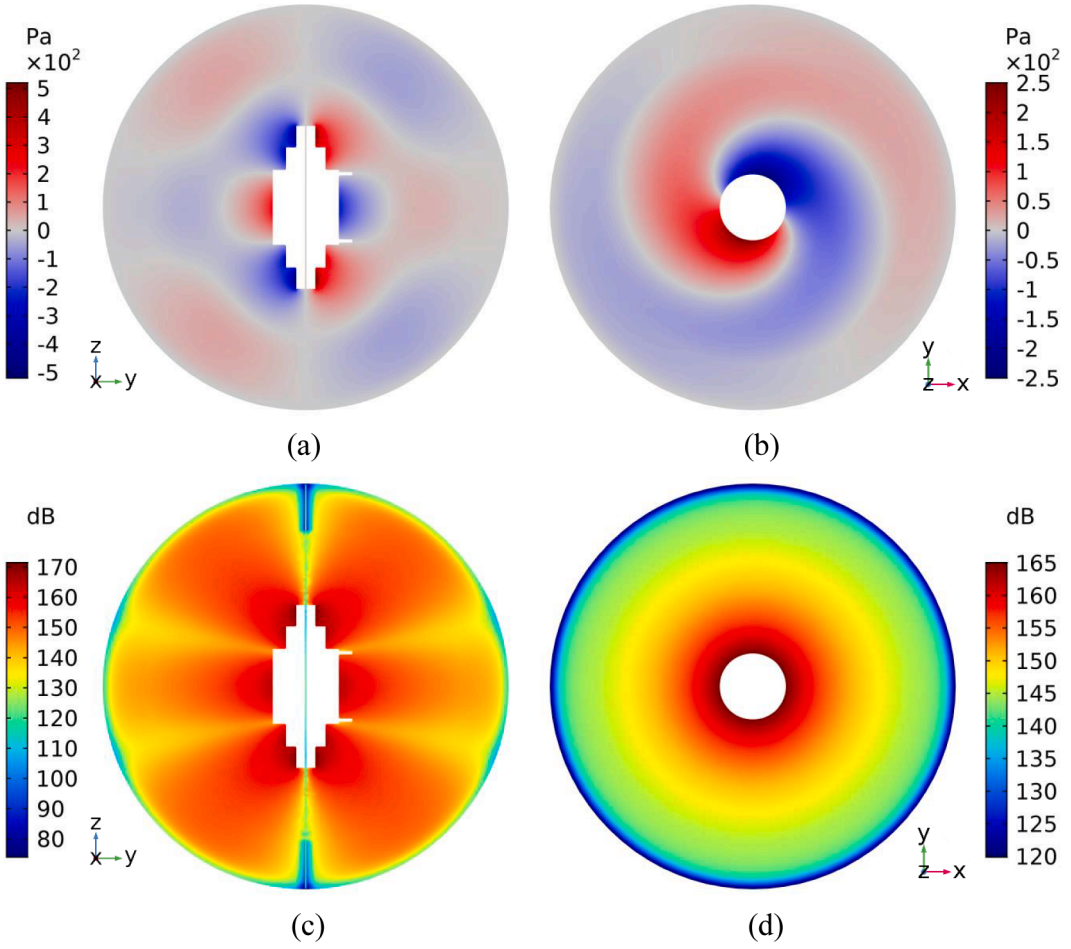

Fig. 7. Sound properties of the proposed OUAT. Sound field distributions of (a) the Y-Z section and (b) the X-Y section of the simulation model. Sound pressure level of (c) the Y-Z section and (d) the X-Y section of the simulation model.

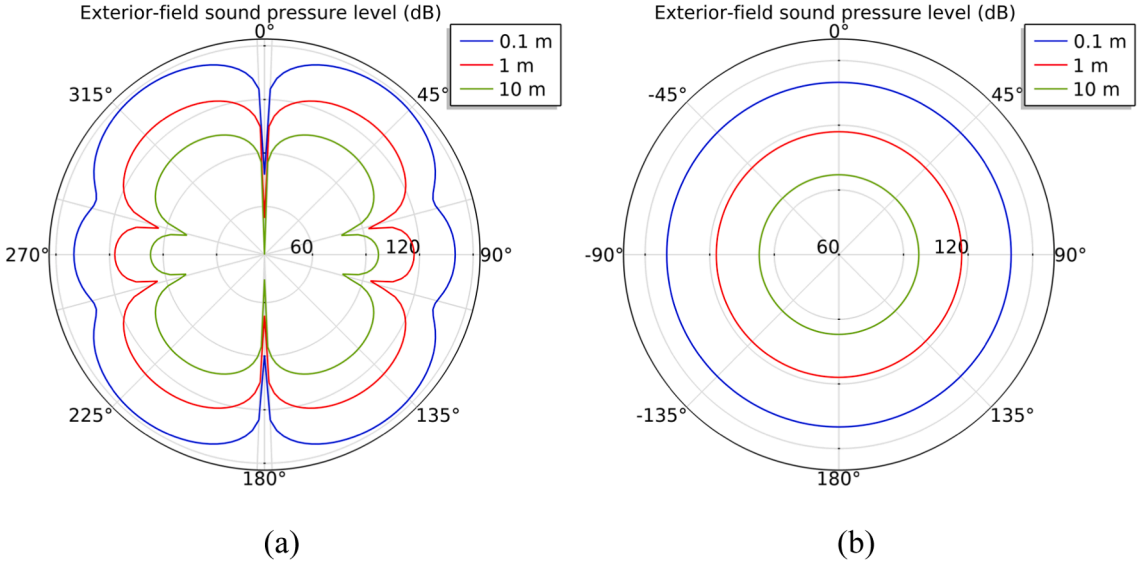

Fig. 8. Ultrasonic irradiation generated by the OUAT at different distances in two planes: (a) Y-Z plane, and (b) X-Y plane.

is the ultrasonic sound pressure amplitude, σ is the surface tension of liquid, K is the heat capacity ration, μ is the liquid viscosity, and ω is the ultrasonic angular frequency.

The radii of the cavitation bubbles located at different positions of the OUAT were calculated to evaluate the cavitation effect produced by the proposed transducer. Ten positions along the axial and

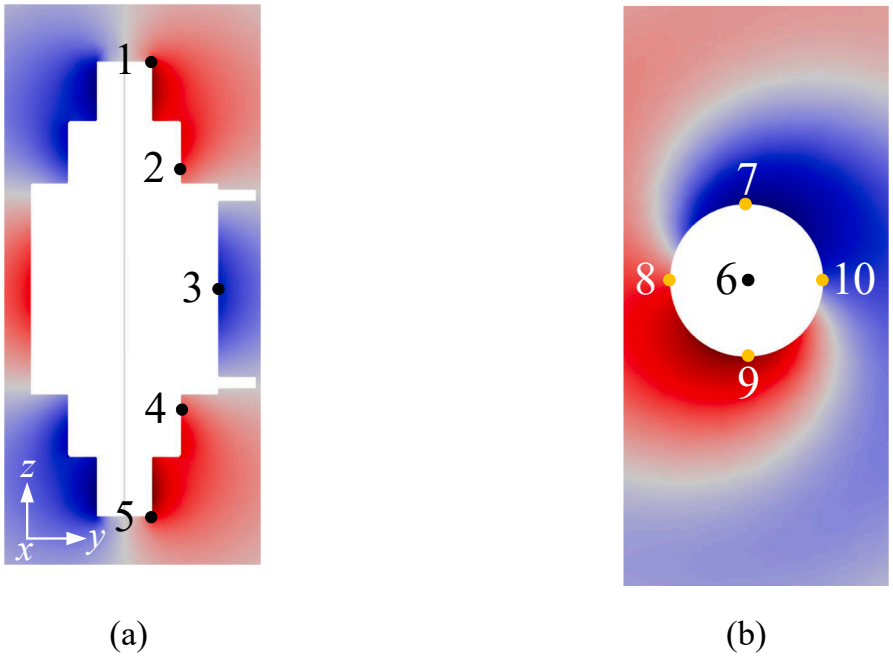

Fig. 9. Extract the sound pressure amplitudes at ten positions in the figure. (a)Axial and (b) circumferential directions of the OUAT.

Table 2
Calculated sound pressure amplitudes of ten positions of the OUAT.

Position	1	2	3	4	5	6	7	8	9	10
Sound pressure amplitude (10^5 Pa)	1.824	1.1	1.2	1.089	1.817	0.955	1.845	1.825	1.85	1.816

Table 3
Values of the factors when calculating the bubble radius.

Factor	ρ (kg/m^3)	σ (N/m)	μ (Pa·s)	c (m/s)	P_0 (10^5Pa)	P_v (Pa)	K	F (kHz)
Value	1000	0.076	0.01	1481	1.013	3.271	1.33	20.173

circumferential directions of the OUAT were selected, as shown in Fig. 9. During the cavitation bubble simulation, the sound field generated by the OUAT was first calculated when the electrical signals with 200 V_{pp} were applied to the two groups of PZT plates. Then the sound pressure amplitudes of these ten positions were extracted, as listed in Table 2. Since the amplitudes in the two vibration directions of the OUAT are inconsistent (seen in Fig. 5), the sound pressure amplitudes of two symmetrical positions on the transducer (such as the positions 1 and 5) are not the same. Finally, the extracted sound pressure amplitudes were substituted into Eq. (15) as the single variable to calculate the cavitation bubble radius.

The Runge-Kutta method was employed in MATLAB to calculate the instantaneous radius of the bubble at these ten positions. The initial conditions at time $t = 0$ were set as follows: $R = R_0$ and $\dot{R} = 0$. Besides, the values of other factors are presented in Table 3. During the calculations, the alternating sound fields were applied in the order of the negative pressure first and then the positive pressure.

The simulation results are illustrated in Fig. 10. The horizontal axis represents an alternating period T of the sound field, and the vertical axis represents the ratio of the instantaneous radius of the bubble to its initial radius. It can be seen that the bubble radii increased rapidly under the negative pressure, and then decreased sharply under the positive pressure. In addition, the bubbles expanded first and then shrunk and rebounded in one period. R/R_0 gradually approaching 0 indicates that the cavitation bubbles were about to collapse. Since the threshold condition for bubble collapsing was not considered in the calculation process, this ratio was not equal to 0. Comparing these ten curves, it can be found that the greater the sound pressure around the bubble, the more intense the growth and collapse of the bubble. In the axial direction of the transducer, the cavitation effects of the bubbles at both ends of the OUAT are the most significant, as shown in Fig. 10(a). And the bubble cavitation effects at the circumference of the OUAT are the most significant, and their effect are similar, as shown in Fig. 10(b). This indicates that the proposed transducer can produce a uniform cavitation effect in the circumferential direction, which further proves the correctness of the proposed omnidirectional ultrasonic removal system for M. aeruginosa.

4. Experiments and discussion

4.1. Fabrication and characterization

After a series of parameters adjustments to maximize the vibration amplitude of transducer, the optimized geometrical parameters of the proposed OUAT were determined, as shown in Fig. 11. Then the OUAT prototype was manufactured and assembled. And an experimental platform based on a 3D laser Doppler vibrator (PSV500-3D-M, Polytec, Germany) was built for testing the vibration characteristics of the OUAT prototype, as shown in Fig. 12. During tests, an end face of the OUAT prototype was used to receive and reflect the laser beam emitted by the

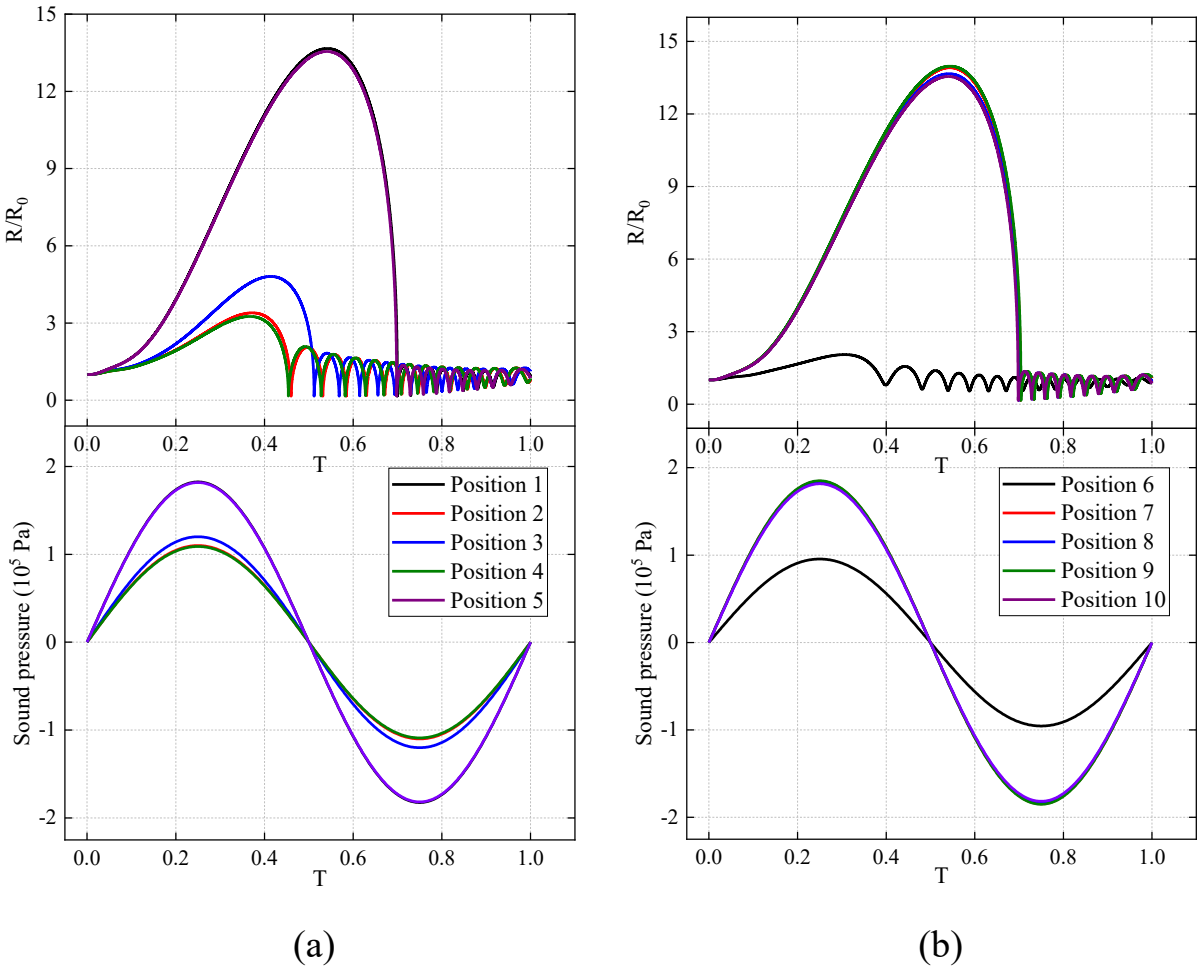

Fig. 10. Variation of the bubble radius and sound pressure in one cycle (T) at different positions of the OUAT in the (a) axial and (b) circumferential directions.

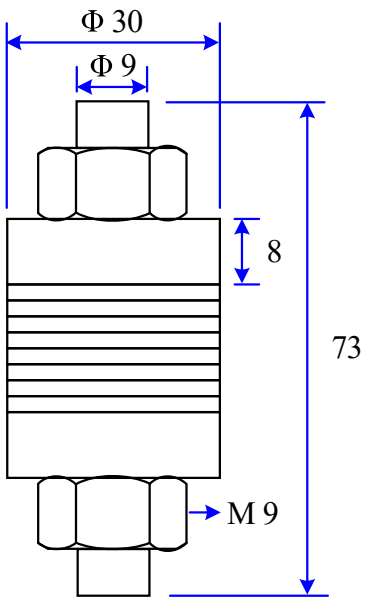

Fig. 11. Geometric parameters of the OUAT.

3D laser Doppler vibrometer.

First, the two first-order bending vibration modes of the OUAT prototype were tested by frequency sweep, respectively (each measurement only one electrical signal was applied to a group of PZT plates), and the test results are shown in Fig. 13. The end face of the transducer performs reciprocating motions in two directions in the X-Y plane, and the two directions of the vibration are almost perfectly orthogonal in space, which is consistent with the simulation results (seen in supporting information named “5” and “6”). However, the measured resonance frequencies of the mode A and mode B of the OUAT prototype in the air are 19613 Hz and 19472 Hz, respectively. There is a frequency difference of 141 Hz between the two vibration modes, and the differences between the measured frequency and the calculated results by FEM are 693 Hz and 578 Hz, respectively. The difference between the measured and the calculated frequencies is primarily due to the fact that the simulation was done in water and the measurements were taken in air. In addition, the assembling error of the prototype and the material error between simulation and reality also caused the frequency differences.

Then applied the same electrical signal to the two groups of PZT plates for the sweep frequency measurement. The frequency response curves of the OUAT prototype measured and calculated by experiment and FEM are shown in Fig. 14. In this case, both curves have only one peak, indicating that the two vibration modes are well coupled when the whole prototype is measured and calculated. After that, the fixed frequency vibration experiment was carried out. Two electrical signals with the same frequency of 19594 Hz and a temporal phase difference of

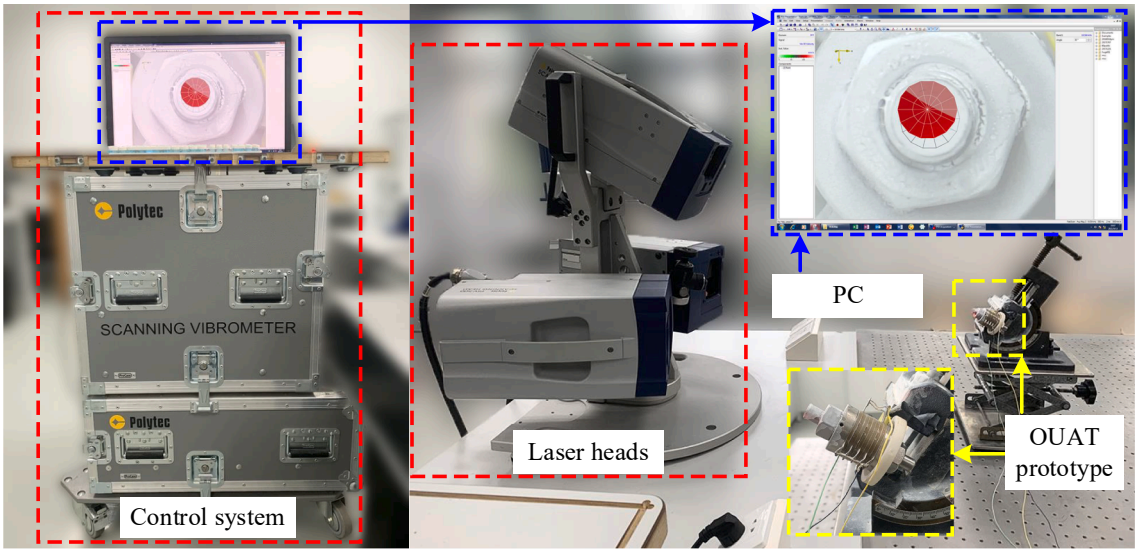

Fig. 12. Experimental platform for measuring the vibration characteristics of the OUAT prototype.

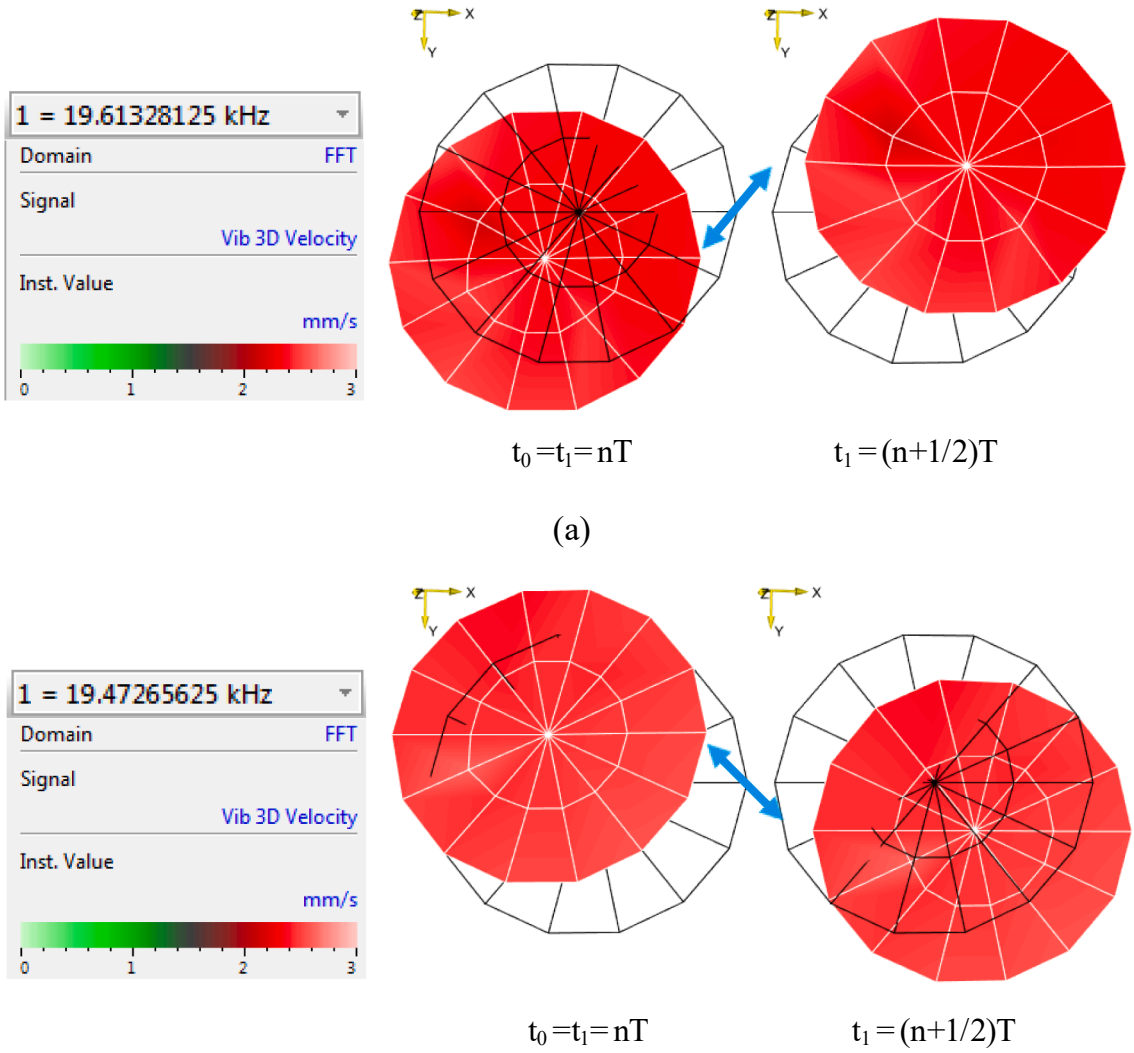

Fig. 13. Measured two bending vibration shapes of the OUAT end face. (a) Mode A. (b) Mode B.

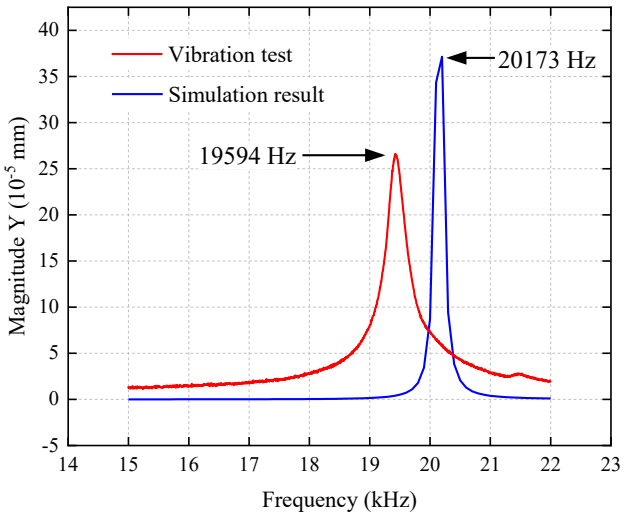

Fig. 14. Frequency response curves of the OUAT prototype computed by the FEM and measured by the 3D laser Doppler vibrometer.

π/2 were simultaneously applied to the two groups of PZT plates, and the end face of the OUAT prototype performed a shaking-head motion in the X-Y plane, as shown in Fig. 15. It can be clearly noted that the measured results are basically consistent with the calculated results, verifying the correctness of the OUAT working principle.

Since the actual working environment of the OUAT is underwater, the resonant frequency in the air may not be the best frequency in its actual work. To maximum the ultrasonic irradiation generated by the transducer, an impedance analyzer (PV80A, Bandera Electronics Corp, China) was used to measure the impedance characteristics of the OUAT prototype in the water environment, as shown in Fig. 16. Applied the same electrical signal to the two groups of PZT plates, the impedance–frequency curve of the transducer in the range of 15,000 Hz to 22,000 Hz was obtained, as shown in Fig. 17. The resonant frequency of OUAT prototype in water is 19,138 Hz, which has reduced by 456 Hz compared with that in air. The reason for the shifting of the resonance frequency is that the coupling effect between solid and liquid in the water environment changes the boundary conditions of the OUAT. The measured frequency of 19,138 Hz is the working frequency of the OUAT prototype in the subsequent algae removal experiments.

4.2. Growth inhibition experiment

In this study, M. aeruginosa, provided by the Shanghai Guangyu Biological Technology Co., Ltd., was used for experiment. Before the experiment, M. aeruginosa was placed in the sterilized culture medium, and then transferred to a light incubator at a constant temperature of 25 ℃ for a 12-hour light–dark illumination cycle to simulate the natural day and night cycle.

The omnidirectional ultrasonic removal experimental system for M. aeruginosa is shown in Fig. 18. When the system begins working, two electrical signals with the same frequency are sent out by a signal

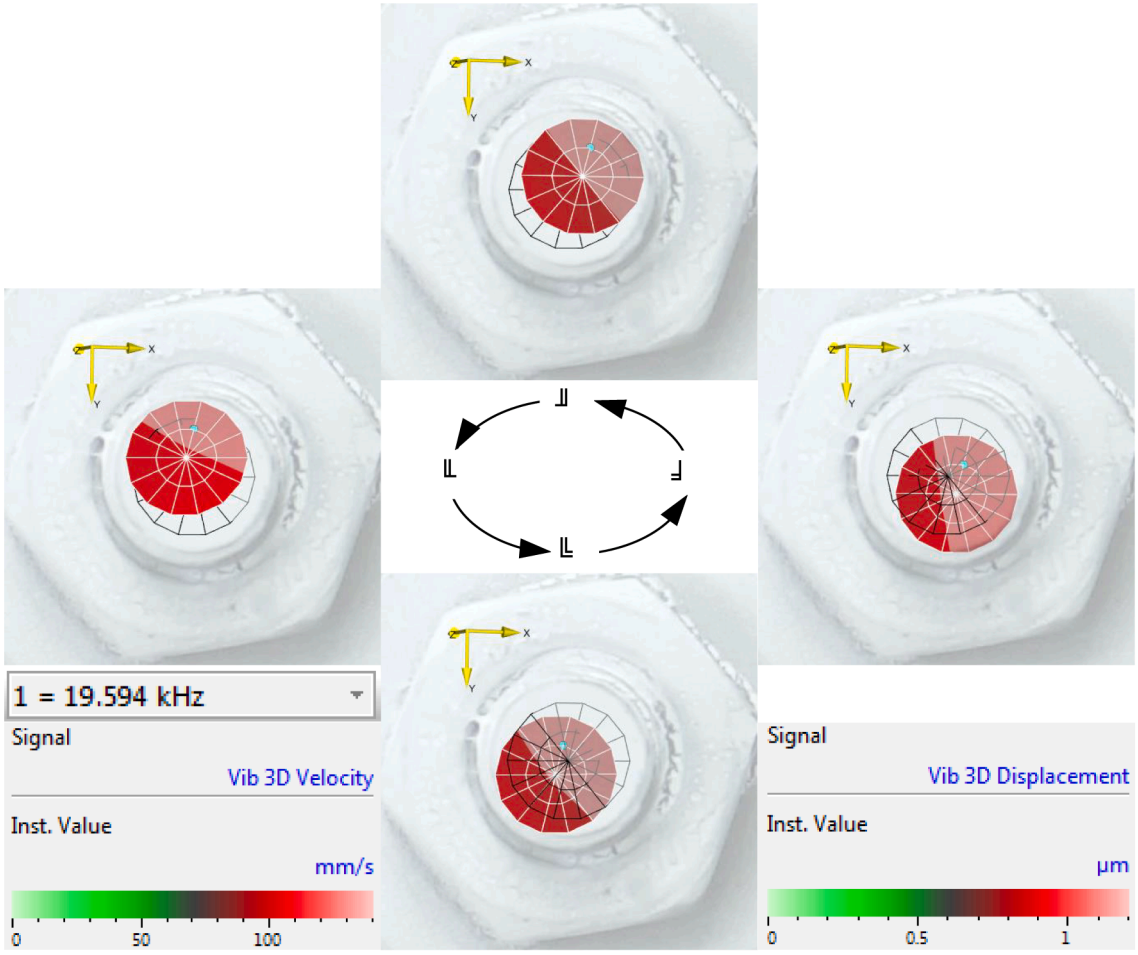

Fig. 15. Shaking-head vibrating motion of the OUAT prototype end face measured by the 3D laser Doppler vibrometer. The measured motion video can be seen in supporting information named "7".

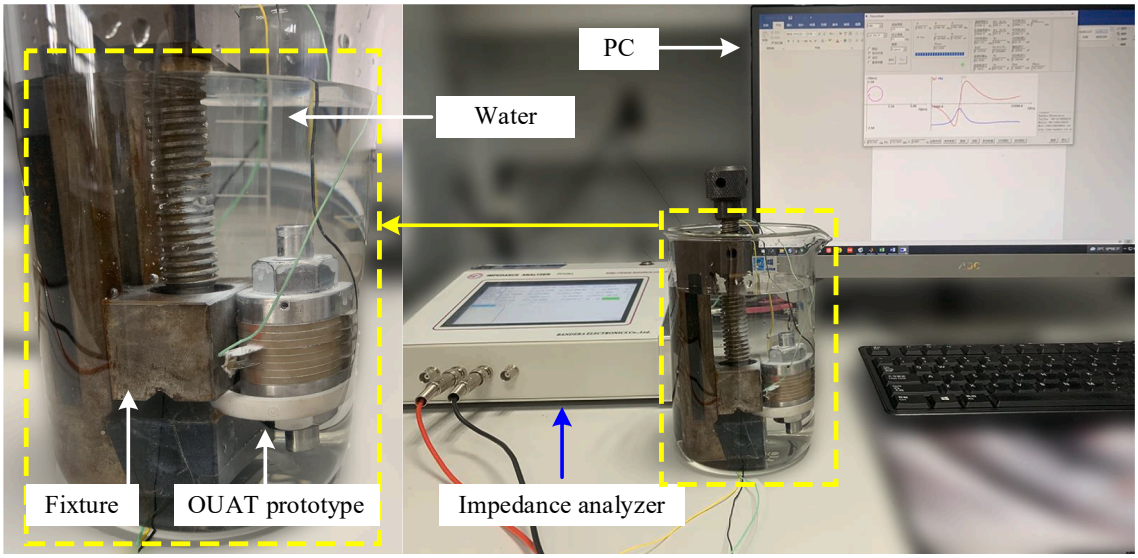

Fig. 16. Experimental device for measuring the impedance characteristics of the OUAT prototype placed in water.

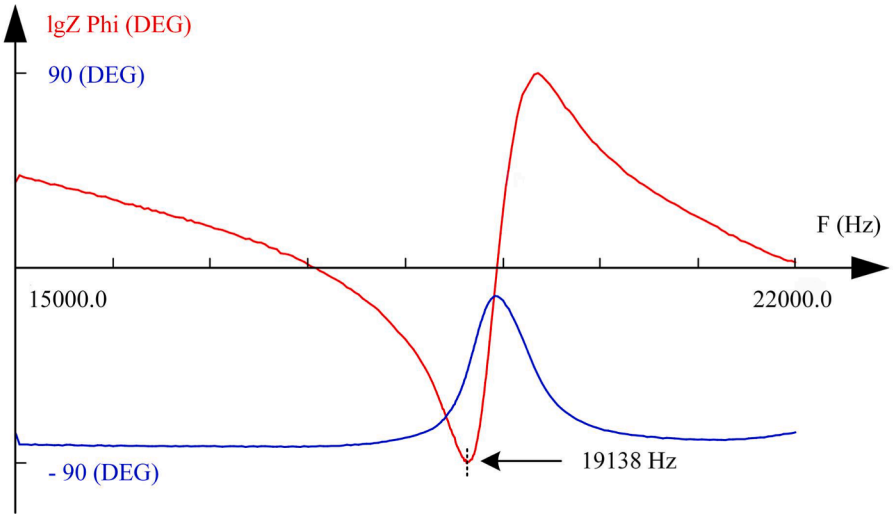

Fig. 17. Impedance measurement results. The red line is the logarithmic value curve of impedance amplitude, and the blue line is the impedance phase curve.

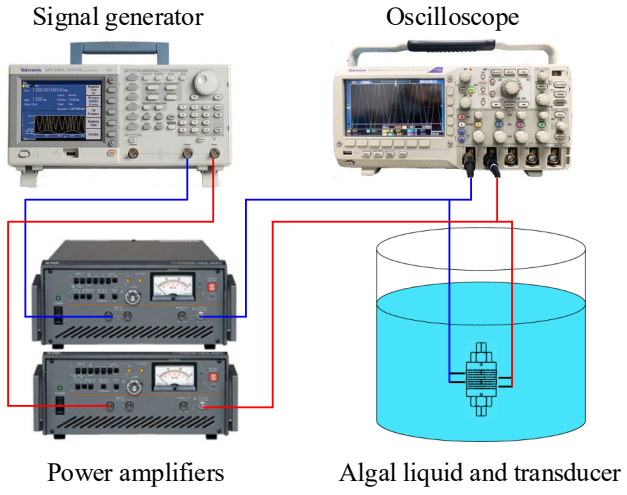

Fig. 18. Omnidirectional ultrasonic removal experimental system for M. aeruginosa.

generator (AFG3022B, Tektronix, USA). The electrical signals are linearly amplified by two power amplifiers (HSA4052, NF, Japan) to the same voltage and then are transmitted to the OUAT and an oscilloscope (DPO2014, Tektronix, USA).

In the ultrasonic removal experiments for M. aeruginosa, a control group and two experimental groups were set up. The algae fluid in the control group grew spontaneously without applying ultrasonic irradiation. Ultrasonic irradiation with different ultrasonic densities were applied to the two experimental groups, and each experimental group contained devices as shown in Fig. 18. Ultrasonic density was measured by the heat quantity method [41-44], which was calculated as:

$$U_D = \left(\frac{dT}{dt} C_p M\right) \Big/ V$$

where U_D is ultrasonic density (W/mL), T is the temperature of treated liquid (℃), t is exposure duration (second), $C_p = 4.2 \times 10^3$ (J/kg/℃) is the specific heat capacity of water at 25 ℃, M is the mass of water (kg), and V is the volume of treated liquid (mL).

The algal density is considered to be the basic indicator for evaluating the growth of M. aeruginosa. In the experiment, it was detected by

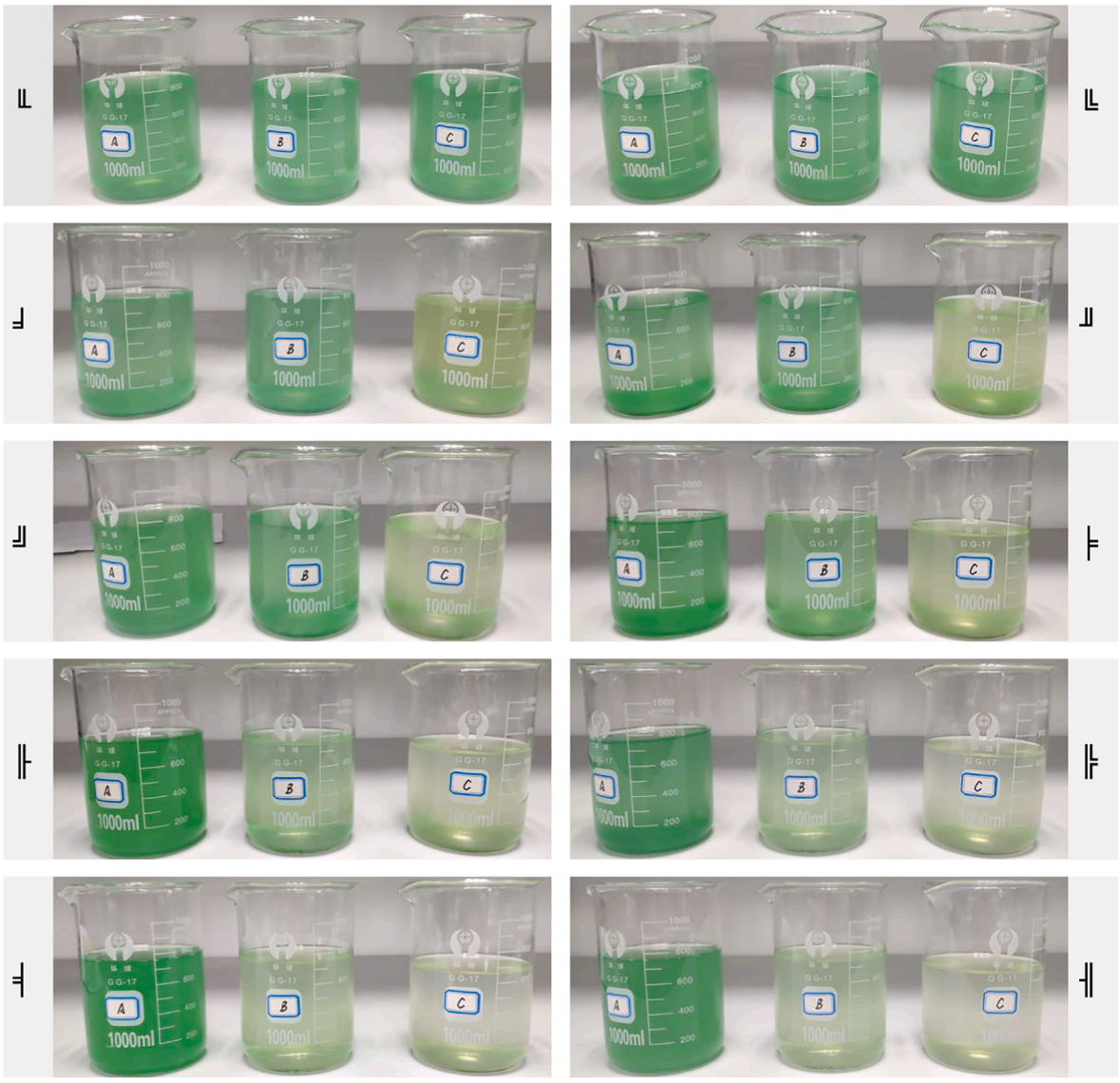

Fig. 19. Growth of M. aeruginosa after treatment at different ultrasonic densities within 10 days. Group A is the control group without ultrasound treatment. Groups B and C are the experimental groups with applied an ultrasonic density of 0.014 W/mL and 0.021 W/mL, respectively.

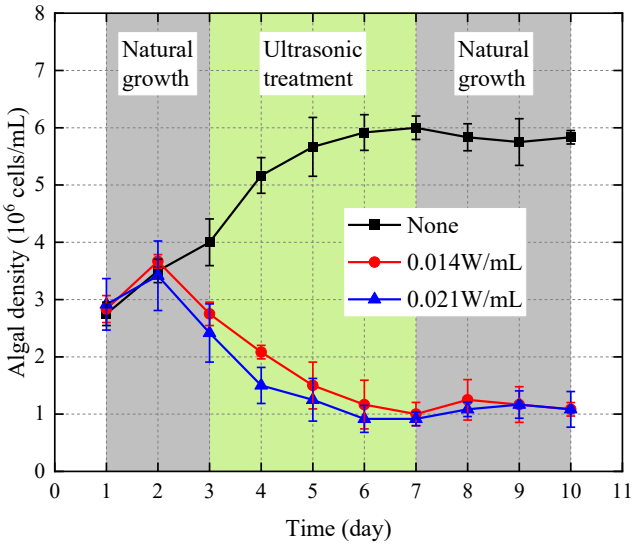

Fig. 20. Concentrations of M. aeruginosa after treatment at different ultrasonic densities.

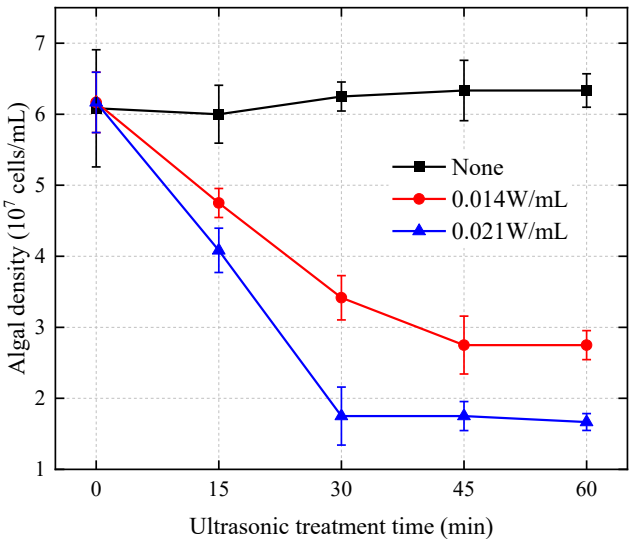

Fig. 23. Change of M. aeruginosa density with ultrasonic treatment time.

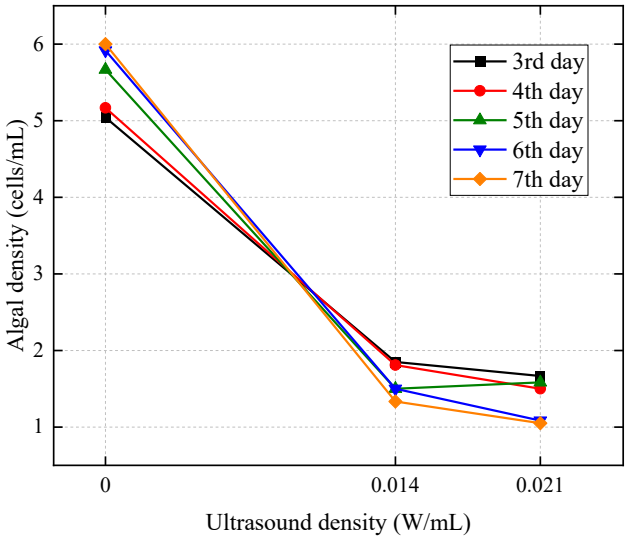

Fig. 21. Means plots of algae densities in different ultrasound irradiation.

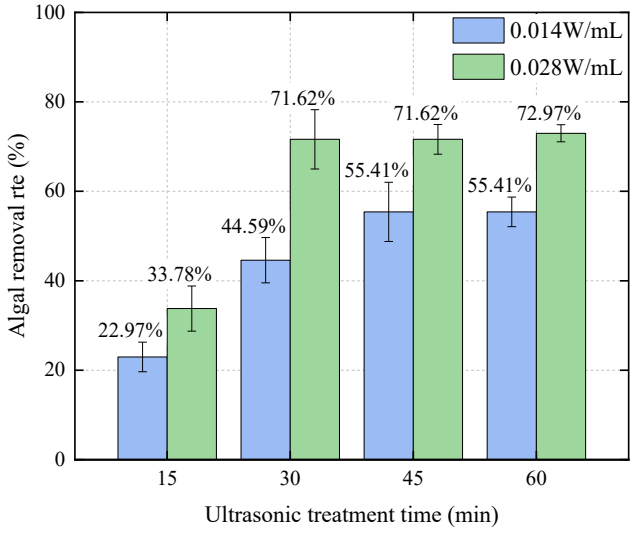

Fig. 24. M. aeruginosa removal rate of different ultrasonic treatment time.

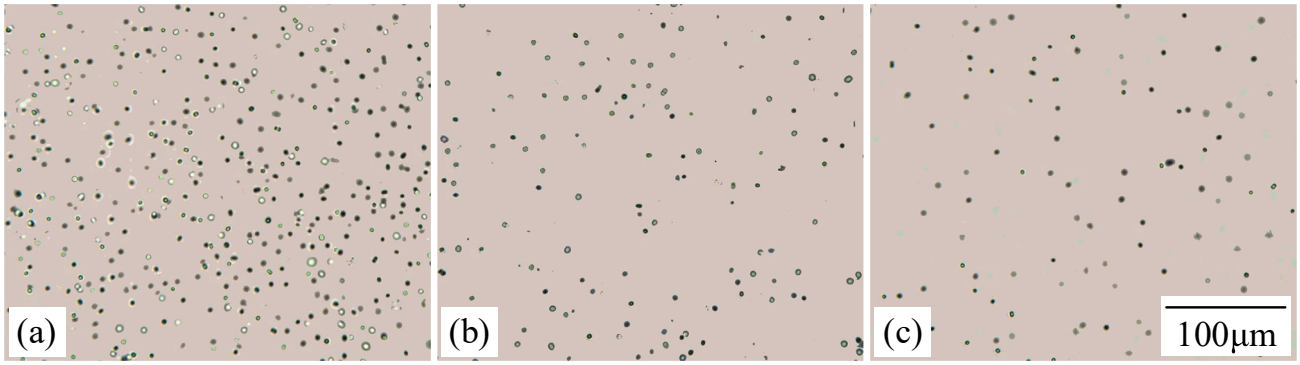

Fig. 22. M. aeruginosa in the field of biological microscope at different ultrasonic densities. (a) Control group, (b) 0.014 W/mL, and (c) 0.021 W/mL.

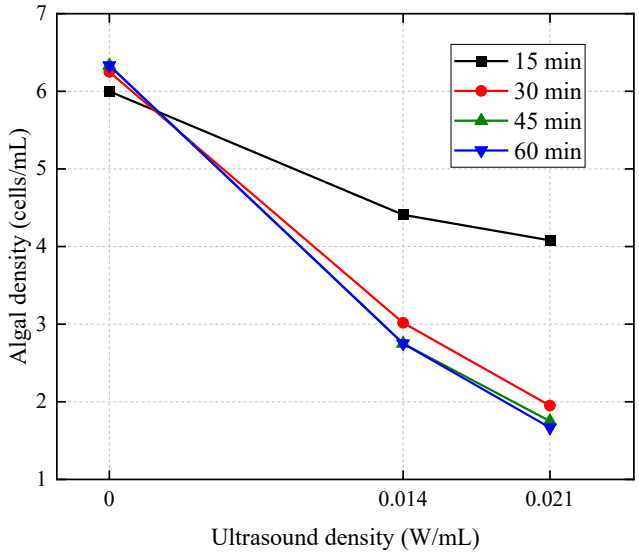

Fig. 25. Means plots of algae densities in different ultrasound irradiation.

a hemocytometer with the aid of an optical microscope (CX40, Shunyu, China), an image sensor (M3LY500TFS, Sony, Japan), and a computer. The M. aeruginosa sank to the bottom of the container when its vesicles was destroyed, which results in different algae densities in waters of different heights. To ensure the accuracy of the detection, samples were collected at the same height from the liquid surface. In addition, the M. aeruginosa liquid at five positions on the same horizontal plane was collected and detected for each experiment, and the five detection results were averaged. The algal cell density was calculated as follows:

$$D = \frac{A}{A_0} \times m \times y \times 10^4 \tag{17}$$

where D is the cell density (cells/mL), A is the area of the counting box (mm^2), A_0 is the counting area (mm^2), m is the number of cells in the counting area, y is the dilution factor of the algal samples, and the volume of the counting box is 0.1 mL.

The algae remove rate was used to characterize the removal effect of the omnidirectional ultrasonic removal system for M. aeruginosa, calculated as.

$$RR = \frac{D_C - D_E}{D_C} \times 100\%$$

where RR represents the removal rate (%), and D_C and D_E denote the algal cell densities of the control group and experimental group at the same time, respectively.

A ten-day growth inhibition experiment of M. aeruginosa was carried out first. Before the experiment, the M. aeruginosa in the same batch was diluted by the same multiple and placed in equal volumes in three beakers labeled A, B, and C. Among them, group A is the control group, and groups B and C are experimental groups. Group A did not receive the ultrasonic irradiation for ten days, and groups B and C did not receive ultrasonic treatment for the first two days. From the 3rd to the 7th days, the experimental groups B and C were treated with ultrasonic irradiation for 20 min at 16:00 every day. During the treatment process, the ultrasonic density applied to the two experimental groups was 0.014 W/mL and 0.021 W/mL, respectively. The growth inhibition experiment was repeated three times to ensure the accuracy of the algal density.

The experimental results as shown in Fig. 19. It can be seen intuitively that the color of the M. aeruginosa liquid in beakers changed over time. The change of color is caused by the destruction of the chloroplasts, which can indicate the variation of the algal density. For the first two days, the liquid color of the three breakers was almost the same green. After ultrasonic irradiation was applied to the two experimental groups on the third day, the liquid color in group C changed significantly, and there was no noticeable change in groups A and B. The difference in this result indicates that the proposed OUAT can quickly inhibit the growth of M. aeruginosa in a short time under the appropriate ultrasonic irradiation intensity. For the 3rd to 7th days, the color of algal liquid in group A became darker gradually than that of the first two days. Meanwhile, the algal liquid color in groups B and C gradually became transparent. The significant color difference indicates that the proposed OUAT can effectively inhibit the growth of M. aeruginosa to a certain extent, achieving the purpose of algal removal and water purification. The ultrasonic irradiation applied to the experimental groups B and C was stopped on the 8th to 10th day. There was little change in the algal liquid color in the two beakers, suggesting that the M. aeruginosa damaged by ultrasonic irradiation from the proposed OUAT did not have the ability to self-repair.

A one-way repeated measurement ANOVA of the algal density obtained from the repeated experiments was first carried out. And the analysis result of the P-value of the Test of Within-Subjects Effects is greater than 0.05, which means that there was no significant difference in the repeated experiments (seen in Tables 4 and 5 in the Appendices A). Then, the algal densities of the three experiments were averaged, and a line graph of density changes of M. aeruginosa within ten days was obtained, as shown in Fig. 20. For the control group A, the M. aeruginosa grew rapidly in the first five days, as well as the growth and reproduction rate of algal tended to be stable due to the limited consumption of inorganic salts (such as nitrogen, phosphorous, etc.) in the algal liquid. For experimental groups B and C, after four days of ultrasonic irradiation of the M. aeruginosa, the algal density decreased from 3.67×10^6 cells/mL and 3.51×10^6 cells/mL to 1.02×10^6 cells/mL and 0.92×10^6 cells/mL, respectively, which proved the effectiveness of the proposed ultrasonic removal system for M. aeruginosa. The density of M. aeruginosa did not rebound significantly when the transducer stopped working in the last two days, indicating that ultrasonic irradiation has a continuous inhibitory effect on the M. aeruginosa growth, verifying that the proposed OUAT has the ability to remove M. aeruginosa and purify water.

To obtain the statistical significance of the algae removal with varying ultrasonic irradiation, a one-way ANOVA was performed. Since the algal fluid was not sonicated for the first two days and the last three days in the growth inhibition experiment, only the experimental results from 3rd to 7th days were analyzed. And the analysis result of the P-value of the Multiple Comparisons is <0.05, indicating that there are significant differences between the group A and the groups B as well as C (seen in Tables 6–8 in the Appendices B). The mean algal densities of different experimental times and different ultrasonic irradiations obtained by the one-way ANOVA in a line graph were plotted, as shown in Fig. 21. It can be concluded that the effect of algae removal is the most significant when the ultrasonic density is 0.021 W/mL.

4.3. Rapid elimination experiment

A rapid elimination experiment of M. aeruginosa was carried out to evaluate the algae removal effect of the proposed removal system in a short time. In this experiment, two experimental groups were irradiated with the ultrasonic density of 0.014 W/mL and 0.021 W/mL, respectively. The ultrasound treatment time for algal liquid is generally 0–20 min with an ultrasound density of 0.01–0.32 W/mL [20,38,45]. Since the ultrasound density used in this experiment is small, the algal liquid in the experiment was irradiated continuously for 60 min. The rapid

elimination experiment was repeated three times to ensure the accuracy of the experimental data. To visualize the process of removing algae, the M. aeruginosa liquid was sampled and counted by an optical microscope every 15 min. Each experiment sampled the algal liquid at five locations on the same horizontal surface and averaged the five calculation results. Compared with the control group, the number of M. aeruginosa cells in the two experimental groups significantly reduced after 60 min of ultrasonic treatment, as shown in Fig. 22.

A one-way repeated measurement ANOVA of the algal density obtained from the repeated experiments was first performed. And the analysis result indicated that there was no significant difference in the repeated experiments ($P > 0.05$, seen in Tables 9 and 10 in the Appendices C). Then, the algal densities of the three experiments were averaged, and a line graph of density changes of M. aeruginosa within 60 min was obtained, as shown in Fig. 23. The experimental data indicated that the densities of M. aeruginosa in the experimental groups with an ultrasonic density of 0.014 W/mL and 0.021 W/mL decreased sharply within 45 min and 30 min, respectively. The algal removal rates of the two ultrasonic densities reached 44.59% and 71.62% at 30 min, respectively, as shown in Fig. 24, which preliminarily verified the fast and efficient algal removal ability of the OUAT. Finally, after 60 min of ultrasonic irradiation, the algal removal rates at the two ultrasonic densities reached 55.41% and 72.97%, respectively, which were only 10.82% and 1.35% higher than that at 30 min. This illustrates that higher ultrasonic density corresponded to higher removal rates, as well as the optimal working time of the OUAT is 30 min in terms of the energy utilization rate of algal removal. These experiment results confirmed the M. aeruginosa removal ability of the OUAT prototype.

Similarly, a one-way ANOVA was performed to obtain the statistical significance for the rapid elimination of M. aeruginosa with varying ultrasonic irradiation. The analysis result of the *P*-value of the Multiple Comparisons is <0.05, indicating that there are significant differences between the group A and the groups B as well as C (seen in Tables 11–13 in the Appendices D). The mean algal densities of different experimental times and different ultrasonic irradiations obtained by the one-way ANOVA in a line graph were plotted, as shown in Fig. 25. It can be concluded that the effect of algae removal is the most significant when the ultrasonic density is 0.021 W/mL.

5. Conclusions

In this paper, a novel omnidirectional ultrasonic cavitation removal system with an ultrasonic transducer for M. aeruginosa is designed, theoretically analyzed, numerically simulated, and experimentally evaluated. Benefiting from the shaking-head movement coupled with the two orthogonal bending vibration modes, the proposed OUAT produces the uniform ultrasonic irradiation in its circumferential direction for omnidirectional removal of M. aeruginosa. This significantly reduces the required number of transducers, simplifies the system configuration, lowers the system cost, and improves the algae-removal efficiency.

Firstly, the correctness of the proposed principle of omnidirectional ultrasonic irradiation was verified by a series of simulations. The sound field generated by both ends of the OUAT rotated and changed along the direction of its shaking-head. The sound pressure level isolines at different distances from the OUAT presented a perfect circular distribution in its circumferential direction, proving the proposed transducer has the function of omnidirectional ultrasonic irradiation. Meanwhile, the bubble cavitation effects at both ends of the OUAT were the most significant, and the cavitation effects in the circumferential direction of the OUAT were consistent, which verifies the correctness of the proposed omnidirectional algae removal principle. Then, the vibration test results illustrated that the shaking-head motion can be perfectly coupled at both ends of the OUAT prototype. Finally, the removal effect of the proposed removal system was evaluated through the removal experiments on the M. aeruginosa. The results of the ten-day growth inhibition experiment exhibited that the M. aeruginosa damaged by ultrasonic irradiation from the OUAT prototype did not have the ability to self-repair. The rapid elimination experimental results indicated that the algal removal rates reached 55.41% and 72.97% after 30 min ultrasonic when the corresponding ultrasonic densities were 0.014 W/mL and 0.021 W/mL, respectively. These results proved the feasibility and effectiveness of the proposed omnidirectional ultrasonic removal system for M. aeruginosa. Certainly, the proposed system is also suitable for the removal of all algae. The kind of omnidirectional algae removal based on a single transducer significantly simplifies the configuration, reduces energy consumption, and has a potential application in algae removal.

CRediT authorship contribution statement

Hao-Ren Feng: Conceptualization, Methodology, Software, Investigation, Writing – original draft. **Jian-An Wang:** Conceptualization, Formal analysis, Validation, Data curation, Visualization. **Liang Wang:** Conceptualization, Funding acquisition, Resources, Supervision, Writing – review & editing. **Jia-Mei Jin:** Visualization, Writing – review & editing. **Shu-Wen Wu:** Software, Validation. **Charles-C. Zhou:** Resources, Supervision.

Declaration of Competing Interest

The authors declare that they have no known competing financial interests or personal relationships that could have appeared to influence the work reported in this paper.

Acknowledgments

This work is supported by the National Natural Science Foundation of China (Grant Nos. U2037603, and 51905262), the Natural Science Foundation of Jiangsu Province (Grant No. BK20190398), the Research Fund of State Key Laboratory of Mechanics and Control of Mechanical Structures (Nanjing University of Aeronautics and astronautics) (Grant Nos. MCMS-I-0320K01, and MCMS-I-0320Y01), the Fundamental Research Funds for the Central Universities (No. NT2021001), and the Guangdong Basic and Applied Basic Research Foundation (No. 2019B1515120017).

Appendix

Appendix A

Table 4
Mauchly's Test of Sphericity of the three repeated growth inhibition experiments.

Experimental group	Within Subjects Effect	Mauchly's W	Approx. Chi-Square	df	*P*/(Sig.)	Greenhouse-Geisser
Group A	Algal Density	0.941	0.484	2	0.785	0.945
Group B	Algal Density	0.955	0.372	2	0.830	0.957
Group C	Algal Density	0.938	0.512	2	0.774	0.942

*Group A: Non ultrasound irradiation. Group B: 0.014 W/mL. Group C: 0.021 W/mL.

Table 5
Test of Within-Subjects Effects of the three repeated growth inhibition experiments.

Experimental group	Sorurce	Type III Sum of Squares	df	Mean Square	F	P/Sig.
Group A	Sphericity Assumed	0.517	2	0.258	1.904	0.178
Group B	Sphericity Assumed	0.163	2	0.081	0.761	0.481
Group C	Sphericity Assumed	0.129	2	0.065	0.635	0.541

Appendix B

Table 6
Test of Homogeneity of Variances of the data from the growth inhibition experiments.

Experiment time	Source	Levene Statistic	df1	df2	*P*/Sig.
3rd day	Based on Mean	0.571	2	6	0.593
4th day	Based on Mean	1.217	2	6	0.360
5th day	Based on Mean	1.400	2	6	0.317
6th day	Based on Mean	2.261	2	6	0.185
7th day	Based on Mean	1.939	2	6	0.224

Table 7
ANOVA of the data from the growth inhibition experiments.

Experiment time	Sum of Squares	df	Mean square	F	*P*/Sig.
3rd day	4.181	2	2.090	15.842	0.04
4th day	23.292	2	11.646	153.455	<0.001
5th day	34.042	2	17.021	76.594	<0.001
6th day	43.042	2	21.521	182.294	<0.001
7th day	46.361	2	23.180	322.197	<0.001

Table 8
Multiple Comparisons by Tukey HSD of the data from the growth inhibition experiments.

Experiment time	Group (I)	Group (J)	Mean Difference (i-J)	Std. Error	*P*/Sig.
3rd day	Group A	Group B	1.25	0.29659	0.013
		Group C	1.58333	0.29659	0.04
4th day	Group A	Group B	3.08333	0.22567	<0.001
		Group C	3.66667	0.22567	<0.001
5th day	Group A	Group B	4.16667	0.38490	<0.001
		Group C	4.08333	0.38490	<0.001
6th day	Group A	Group B	4.16667	0.28054	<0.001
		Group C	4.08333	0.28054	<0.001
7th day	Group A	Group B	4.66667	0.21900	<0.001
		Group C	4.95000	0.21900	<0.001

Appendix C

Table 9
Mauchly's Test of Sphericity of the three repeated rapid elimination experiments.

Experimental group	Within Subjects Effect	Mauchly's W	Approx. Chi-Square	df	*P*/(Sig.)	Greenhouse-Geisser
Group A	Algal Density	0.238	4.302	2	0.116	0.568
Group B	Algal Density	0.645	1.314	2	0.528	0.738
Group C	Algal Density	0.473	2.244	2	0.326	0.655

Table 10
Test of Within-Subjects Effects of the three repeated rapid elimination experiments.

Experimental group	Sorurce	Type III Sum of Squares	df	Mean Square	F	*P*/Sig.
Group A	Sphericity Assumed	0.111	2	0.055	3.194	0.096
Group B	Sphericity Assumed	0.002	2	0.001	0.058	0.944
Group C	Sphericity Assumed	0.021	2	0.011	1.340	0.315

Appendix D

Table 11
Test of Homogeneity of Variances of the data from the rapid elimination experiments.

Experiment time	Source	Levene Statistic	df1	df2	*P*/Sig.
15 min	Based on Mean	0.354	2	6	0.715
30 min	Based on Mean	0.516	2	6	0.621
45 min	Based on Mean	1.149	2	6	0.378
60 min	Based on Mean	0.832	2	6	0.480

Table 12
ANOVA of the data from the rapid elimination experiments.

Experiment time	Sum of Squares	df	Mean square	F	*P*/Sig.
15 min	5.681	2	2.840	208.673	<0.001
30 min	31.056	2	15.528	375.684	<0.001
45 min	34.847	2	17.424	636.194	<0.001
60 min	35.792	2	17.896	937.745	<0.001

Table 13
Multiple Comparisons by Tukey HSD of the data from the rapid elimination experiments.

Experiment time	Group (I)	Group (J)	Mean Difference (i-J)	Std. Error	*P*/Sig.
15 min	Group A	Group B	1.25000	0.09526	<0.001
		Group C	1.91667	0.09526	<0.001
30 min	Group A	Group B	2.83333	0.09813	<0.001
		Group C	4.50000	0.09813	<0.001
45 min	Group A	Group B	3.58333	0.11139	<0.001
		Group C	4.58333	0.11139	<0.001
60 min	Group A	Group B	3.58333	0.09329	<0.001
		Group C	4.66667	0.09329	<0.001

References

[1] B. Zhao, X.L. Cai, S. Wang, X.X. Yang, Analysis of the causes of cyanobacteria bloom: a review, J. Resour. Ecol. 11 (4) (2020) 405–413.
[2] P. Rajasekhar, L.H. Fan, T. Nguyen, F.A. Roddick, A review of the use of sonication to control cyanobacterial blooms, Water Res. 46 (14) (2012) 4319–4329.
[3] M.H. Dehghani, Removal of cyanobacterial and algal cells from water by ultrasonic waves - A review, J. Mol. Liq. 222 (2016) 1109–1114.
[4] M.R. Al Shehhi, I. Gherboudj, H. Ghedira, An overview of historical harmful algae blooms outbreaks in the Arabian Seas, Mar. Pollut. Bull. 86 (1–2) (2014) 314–324.
[5] K. Wang, J. Saththasivam, W. Yiming, K. Loganathan, Z.Y. Liu, Fast and efficient separation of seawater algae using a low-fouling micro/nano-composite membrane, Desalination 43 (2018) 108–112.
[6] F. Wu, H. Kong, Y.Y. Shang, Z.Q. Zhou, Y. Gul, Q.G. Liu, M.H. Hu, Histopathological alterations in triangle sail mussel (Hyriopsis cumingii) exposed to toxic cyanobacteria (Microcystis aeruginosa) under hypoxia, Aquaculture 467 (2017) 182–189.
[7] L. Li, N.Y. Gao, Y. Deng, J.J. Yao, K.J. Zhang, Characterization of intracellular & extracellular algae organic matters (AOM) of Microcystic aeruginosa and formation of AOM-associated disinfection byproducts and odor & taste compounds, Water Res. 46 (4) (2012) 1233–1240.
[8] T.J. Lee, K. Nakano, M. Matsumara, Ultrasonic irirradiation for blue-green algae bloom control, Environ. Technol. 22 (4) (2001) 383–390.
[9] C. Svrcek, D.W. Smith, Cyanobacteria toxins and the current state of knowledge on water treatment options: A review, J. Environ. Eng. Sci. 3 (3) (2004) 155–185.
[10] F. Motahari, M.R. Mozdianfard, F. Soofivand, M. Salavati-Niasari, NiO nanostructures: synthesis, characterization and photocatalyst application in dye wastewater treatment, RSC Adv. 4 (53) (2014) 27654.
[11] M. Mousavi-Kamazani, Z. Zarghami, M. Salavati-Niasari, Facile and novel chemical synthesis, characterization, and formation mechanism of copper sulfide (Cu2S, Cu2S/CuS, CuS) nanostructures for increasing the efficiency of solar cells, J. Phys. Chem. C 120 (4) (2016) 2096–2108.
[12] S. Zinatloo-Ajabshir, S. Mortazavi-Derazkola, M. Salavati-Niasari, Simple sono-chemical synthesis of Ho2O3-SiO2 nanocomposites as an effective photocatalyst for degradation and removal of organic contaminant, Ultrason. Sonochem. 39 (2017) 452–460.
[13] M. Sabet, M. Salavati-Niasari, O. Amiri, Using different chemical methods for deposition of CdS on TiO2 surface and investigation of their influences on the dyesensitized solar cell performance, Electrochim. Acta 117 (2014) 504–520.
[14] C.Y. Ahn, M.H. Park, S.H. Joung, H.S. Kim, K.Y. Jang, H.M. Oh, Growth Inhibition of Cyanobacteria by Ultrasonic Radiation: Laboratory and Enclosure Studies, Environ. Sci. Technol. 37 (13) (2003) 3031–3037.
[15] A. Muthupandian, The characterization of acoustic cavitation bubbles - an overview, Ultrason. Sonochem. 18 (4) (2011) 864–872.
[16] J.W. Tang, Q.Y. Wu, H.W. Hao, Y.F. Chen, M.S. Wu, Effect of 1.7 MHz ultrasound on a gas-vacuolate cyanobacterium and a gas-vacuole negative cyanobacterium, Colloids Surf. B Biointerfaces 36 (2) (2004) 115–121.
[17] K.L. Wu, Y. Xing, N. Chu, P. Wu, L.L. Cao, D.Z. Wu, A carrier wave extraction method for cavitation characterization based on time synchronous average and time-frequency analysis, J. Sound Vib. 489 (2020), 115682.
[18] K. Vokurka, Free oscillations of a cavitation bubble, J. Sound Vib. 135 (3) (1989) 399–410.
[19] J.S.M. Rusby, The onset of sound wave distortion and cavitation in water and sea water, J. Sound Vib. 13 (3) (1970) 257-IN3.
[20] Y. Kong, Y.Z. Peng, Z. Zhang, M. Zhang, Y.H. Zhou, Z. Duan, Removal of Microcystis aeruginosa by ultrasound: inactivation mechanism and release of algal organic matter, Ultrason. Sonochem. 56 (2019) 447–457.
[21] G.B. Chen, X.M. Ding, W. Zhou, Study on ultrasonic treatment for degradation of Microcystins (MCs), Ultrason. Sonochem. 63 (2020), 104900.
[22] A. Rodriguez-Molares, S. Dickson, P. Hobson, C. Howard, A. Zander, M. Burch, Quantification of the ultrasound induced sedimentation of Microcystis aeruginosa, Ultrason. Sonochem. 21 (4) (2014) 1299–1304.
[23] G.H.E. LaLiberte, Literature Review of the Effects of Ultrasonic Waves on Cyanobacteria, Other Aquatic Organisms, and Water Quality, Wisconsin Department of Natural Resource, Research Report, 2014.
[24] X. Wu, E.M. Joyce, T.J. Mason, The effects of ultrasound on cyanobacteria, Harmful Algae 10 (6) (2011) 738–743.
[25] H.K. Hudnell, The state of US freshwater harmful algal blooms assessments, policy and legislation, Toxicon 55 (5) (2010) 1024–1034.
[26] O.D. Schneider, L.A. Weinrich, S. Brezinski, Ultrasonic Treatment of Algae in a New Jersey Reservoir, J. Am. Water Works Ass. 107 (10) (2015) E533–E542.
[27] T.J. Lee, K. Nakano, M. Matsumura, A novel strategy for cyanobacterial bloom control by ultrasonic irirradiation, Water Sci. Technol. 46 (6–7) (2002) 207–215.
[28] P. Rajasekhar, L.H. Fan, T. Nguyen, F.A. Roddick, Impact of sonication at 20 kHz on Microcystis aeruginosa, Anabaena circinalis and Chlorella sp, Water Res. 46 (5) (2012) 1473–1481.
[29] Y.R. Huang, H.Z. Li, X.M. Wei, D.H. Wang, Y.T. Liu, L. Li, The effect of low frequency ultrasonic treatment on the release of extracellular organic matter of Microcystis aeruginosa, Chem. Eng. J. 383 (2020), 123141.

[30] T.J. Mason, A.J. Cobley, J.E. Graves, D. Morgan, New evidence for the inverse dependence of mechanical and chemical effects on the frequency of ultrasound, Ultrason. Sonochem. 18 (1) (2011) 226–230.
[31] E.M. Joyce, X.G. Wu, T.J. Mason, Effect of ultrasonic frequency and power on algae suspensions, J. Environ. Sci. Heal. A. 45 (7) (2010) 863–866.
[32] Y.T. Li, X.D. Shi, Z. Zhang, Y.Z. Peng, Enhanced coagulation by high-frequency ultrasound in Microcystis aeruginosa-laden water: strategies and mechanisms, Ultrason. Sonochem. 55 (2019) 232–242.
[33] C. Liu, J. Wang, Z. Cao, W. Chen, H.K. Bi, Variation of dissolved organic nitrogen concentration during the ultrasonic pretreatment to Microcystis aeruginosa, Ultrason. Sonochem. 29 (2016) 236–243.
[34] E.A. Neppiras, Acoustic cavitation, Phys. Rep. 61 (3) (1980) 159–251.
[35] C.E. Brennen, Cavitation and Bubble Dynamics, Cambridge University Press, 2014.
[36] M.O.D. Andrade, S.R. Haqshenas, K.J. Pahk, N. Saffari, Modeling the physics of bubble nucleation in histotripsy, IEEE Trans. Ultrason., Ferroelectr. Freq. Control 68 (2021) 2871–2883.
[37] M.O.D. Andrade, S.R. Haqshenas, K.J. Pahk, N. Saffari, The effects of ultrasound pressure and temperature fields in millisecond bubble nucleation, Ultrasonics – Sonochem. 55 (2019) 262–272.
[38] H.C. Huang, G. Wu, C.W. Sheng, J.N. Wu, D.H. Li, H.Z. Wang, Improved Cyanobacteria Removal from Harmful Algae Blooms by Two-Cycle, Low-Frequency, Low-Density, and Short-Duration Ultrasonic Radiation, Water 12 (9) (2020) 2431.
[39] W.X. Qu, Y.H. Xie, Y. Shen, J. Han, M.Y. You, T. Zhu, Simulation on the effects of various factors on the motion of ultrasonic cavitation bubble, Math. Modell. Eng. Probl. 4 (4) (2017) 173–178.
[40] X. Guo, Y.L. Yang, X. Li, Z.W. Zhou, C.H. Ma, Y. Zhang, Simulation of ultrasound cavitation bubble and numerical/experimental analysis of flocs breakage process, China Environm. Sci. 35 (5) (2015) 1429–1435.
[41] T.J. Mason, J.P. Lorimer, D.M. Bates, Quantifying sonochemistry: casting some light on a 'black art', Ultrasonics 30 (1992) 40–42.
[42] R. Vinay, A. Abbas, Experimental investigations on ultrasound mediated particle breakage, Ultrason. Sonochem. 15 (1) (2018) 55–64.
[43] M. Kurokawa, K.P. King, X.G. Wu, E.M. Joyce, T.J. Mason, K. Yamamoto, Effect of sonication frequency on the disruption of algae, Ultrason. Sonochem. 31 (2016) 157–162.
[44] S. Koda, T. Kimura, T. Kondo, H. Mitome, A standard method to calibrate sonochemical efficiency of an individual reaction system, Ultrason. Sonochem. 10 (3) (2003) 149–156.
[45] P. Rajasekhar, L. Fan, T. Nguyen, F.A. Roddick, Impact of sonication at 20 kHz on Microcystis aeruginosa, Anabaena circinalis and Chlorella sp. Water res. 46 (5) (2012) 1473–1481.